



Low-frequency intensity noise in semiconductor lasers  
by Margaret Manson Hall

A thesis submitted in partial fulfillment of the requirements for the degree of Doctor of Philosophy in  
Physics

Montana State University

© Copyright by Margaret Manson Hall (1996)

Abstract:

Intensity fluctuations (intensity noise) at 25 MHz of two semiconductor lasers are studied experimentally and theoretically. At this frequency two sources of intensity noise can be examined; quantum noise and noise originating from longitudinal mode competition. This latter source of noise occurs when more than one longitudinal mode competes for laser power.

The intensity fluctuations for a free running laser diode (with no external optical feedback) and an external cavity laser (with external optical feedback) are measured as a function of injection current. An experimental value for the shot noise limit (the standard limit predicted by quantum mechanics) is also obtained, and all laser noise measurements are compared with this limit. We find that at twice the threshold injection current, the intensity noise of the free running laser is only 3.5 dB above the shot noise limit, and that of the external cavity laser 5 dB above the shot noise limit.

The ratio of the intensities of the main longitudinal mode to the side longitudinal modes is measured for both lasers, also as a function of injection current. We find that the intensity noise is decreased when the side modes are suppressed.

Single mode semiclassical and fully quantum mechanical theories are used to model the intensity noise. The two theories predict similar levels of intensity noise at low injection currents; at higher injection currents where quantum noise sources not included in the semiclassical theory play a role, the noise predictions of the two theories deviate. In particular, the semiclassical theory predicts noise below the shot noise level at high injection currents, even when the injection current carries the full shot noise.

Both theories generally predict lower levels of intensity noise than that which is measured; the single mode theories do not account for longitudinal mode competition noise. Thus we conclude that longitudinal mode competition is a significant source of intensity noise even when the side modes are suppressed below the main mode more than 30 dB. Thus a multimode theory may be necessary to effectively model the intensity noise of semiconductor lasers.

LOW-FREQUENCY INTENSITY NOISE  
in  
SEMICONDUCTOR LASERS

by

MARGARET MANSON HALL

A thesis submitted in partial fulfillment  
of the requirements for the degree

of

Doctor of Philosophy

in

Physics

MONTANA STATE UNIVERSITY  
Bozeman, Montana

July 1996

D318  
H1435

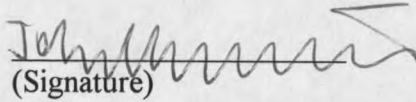
APPROVAL

of a thesis submitted by

Margaret Manson Hall

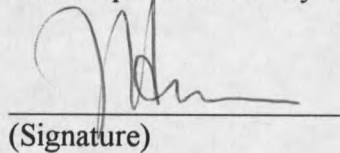
This thesis has been read by each member of the thesis committee and has been found to be satisfactory regarding content, English usage, format, citations, bibliographic style, and consistency, and is ready for submission to the College of Graduate Studies.

Dr. John Carlsten

  
(Signature) 7-18-96  
Date

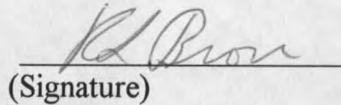
Approved for the Department of Physics

Dr. John Hermanson

  
(Signature) 7-18-96  
Date

Approved for the College of Graduate Studies

Dr. Robert Brown

  
(Signature) 8/4/96  
Date

## STATEMENT OF PERMISSION TO USE

In presenting this thesis in partial fulfillment of the requirements for a doctoral degree at Montana State University-Bozeman, I agree that the Library shall make it available to borrowers under rules of the Library. I further agree that copying of this thesis is allowable only for scholarly purposes, consistent with "fair use" as prescribed in the U.S. Copyright Law. Requests for extensive copying or reproduction of the thesis should be referred to University Microfilms International, 300 North Zeeb Road, Ann Arbor, Michigan 48106, to whom I have granted "the exclusive right to reproduce and distribute my dissertation in and from microfilm along with the non-exclusive right to reproduce and distribute my abstract in any format in whole or in part."

Signature Margaret M. Hall

Date July 18, 1996

## ACKNOWLEDGMENTS

The first and foremost person I would like to thank is my advisor Dr. John Carlsten. Of all his great attributes, I single out his patience as the characteristic I appreciated most.

Dan Kilper and Gregg Switzer helped me immensely. Dan “pushed” me to apply the quantum theory to my work. As a result I learned much more than I ever would have without him, and have a more solid thesis project to show for it. Gregg Switzer was the best lab partner one could ask for. On the practical side, one of the two lasers I used for my project was one that he had built from scratch. He also inspired me by always helping others, and conveying his excitement for physics to undergraduates or anyone who happened to be in the lab.

Others who were there to obtain guidance from and talk with were Jim Wessel, Phil Battle, Tim Heumier, and Kevin Repasky. I also appreciated the time that Eric Anderson and Norm Williams spent with me.

Finally, I would like to thank Rand Swanson for absolutely everything he has done for me. Rand was always there for me; for my physics questions as well as for my “physics” frustrations. This was no easy feat.

## TABLE OF CONTENTS

	Page
1. INTRODUCTION.....	1
Semiconductor Laser Basics.....	3
Intensity Noise Spectrum.....	5
The Shot Noise Limit (SNL).....	8
Recent Research.....	9
2. THE LANGEVIN RATE EQUATIONS.....	12
Semiclassical Langevin Rate Equations.....	13
Quantum Mechanical Langevin Rate Equations.....	19
Pump Noise.....	27
Quantitative Comparison.....	30
3. SEMICONDUCTOR LASER.....	32
Laser Diode.....	32
Laser Intensity Noise Measurements.....	34
Measurement of the Shot Noise Level.....	35
Experimental Precautions Taken.....	37
Measurement of Laser Side Mode Suppression.....	39
Results.....	40
Discussion.....	42
4. EXTERNAL CAVITY SEMICONDUCTOR LASER.....	44
External Cavity Semiconductor Laser.....	45
Experiment.....	50
Results.....	50
Discussion.....	52
5. CONCLUSION.....	54

## TABLE OF CONTENTS--Continued

APPENDICES.....	55
A. Controller Noise.....	56
B. Laser Parameters.....	62
C. The Langevin Diffusion Coefficients.....	71
REFERENCES CITED.....	77

## LIST OF FIGURES

Figure	Page
1.1 Magnitude of laser diode intensity noise.....	2
1.2 Semiconductor laser.....	4
1.3 Longitudinal side modes of a laser diode.....	5
1.4 Intensity noise spectrum.....	6
2.1 Reservoir theory schematic.....	22
2.2 Internal field, external field flux, and reflected external coupling noise operators..	25
2.3 "Constant voltage" and "constant current" driven diode lasers.....	28
2.4 Theoretical intensity noise with and without pump noise.....	30
2.5 Semiclassical and quantum theories.....	31
3.1 Buried double-heterostructure laser diode.....	33
3.2 Experimental setup for measuring the intensity noise.....	34
3.3 The shot noise of an LED and photodiode ac saturation properties.....	36
3.4 Linearity of the photodiode dc response.....	38
3.5 Experimental setup for measuring the longitudinal side mode suppression.....	40
3.6 The measured intensity noise and side mode suppression for the free running laser.....	41
3.7 Theoretical and experimental intensity noise results for the free running laser.....	42

## LIST OF FIGURES--Continued

4.1 Schematic of external cavity semiconductor laser.....	45
4.2 Details of the external cavity semiconductor laser.....	47
4.3 Longitudinal side modes of external cavity laser diode.....	48
4.4 Output power vs. injection current for the free running and external cavity lasers...	49
4.5 The measured intensity noise and side mode suppression of external cavity laser.....	51
4.6 Theoretical and experimental intensity noise results for the external cavity laser.....	52
A.1 Controller noise (0-150 MHz).....	58
A.2 Controller noise (0-15 MHz).....	59
A.3 Controller noise (0-1.5 MHz).....	59
A.4 Battery supply setup.....	60
A.5 GPIB cable configurations.....	61
A.6 GPIB cable noise.....	61
B.1 The number of carriers at transparency.....	66
B.2 Determining the front surface reflectivity of the external cavity.....	69
B.3 Determining the scattering losses of the grating.....	70

## ABSTRACT

Intensity fluctuations (intensity noise) at 25 MHz of two semiconductor lasers are studied experimentally and theoretically. At this frequency two sources of intensity noise can be examined; quantum noise and noise originating from longitudinal mode competition. This latter source of noise occurs when more than one longitudinal mode competes for laser power.

The intensity fluctuations for a free running laser diode (with no external optical feedback) and an external cavity laser (with external optical feedback) are measured as a function of injection current. An experimental value for the shot noise limit (the standard limit predicted by quantum mechanics) is also obtained, and all laser noise measurements are compared with this limit. We find that at twice the threshold injection current, the intensity noise of the free running laser is only 3.5 dB above the shot noise limit, and that of the external cavity laser 5 dB above the shot noise limit.

The ratio of the intensities of the main longitudinal mode to the side longitudinal modes is measured for both lasers, also as a function of injection current. We find that the intensity noise is decreased when the side modes are suppressed.

Single mode semiclassical and fully quantum mechanical theories are used to model the intensity noise. The two theories predict similar levels of intensity noise at low injection currents; at higher injection currents where quantum noise sources not included in the semiclassical theory play a role, the noise predictions of the two theories deviate. In particular, the semiclassical theory predicts noise below the shot noise level at high injection currents, even when the injection current carries the full shot noise.

Both theories generally predict lower levels of intensity noise than that which is measured; the single mode theories do not account for longitudinal mode competition noise. Thus we conclude that longitudinal mode competition is a significant source of intensity noise even when the side modes are suppressed below the main mode more than 30 dB. Thus a multimode theory may be necessary to effectively model the intensity noise of semiconductor lasers.

## CHAPTER 1

### INTRODUCTION

Intensity fluctuations, although often small, are always present in a continuous wave (cw) laser beam. The sources of this "intensity noise" are numerous, and vary with laser type and structure, pumping level, and frequency of the fluctuations. In order to suppress the intensity fluctuations, an understanding of the noise mechanisms in the laser is crucial. An understanding of the fluctuations is also interesting from classical and quantum optical viewpoints.

An off-the-shelf semiconductor laser, operated above threshold, will have optical intensity noise 5 to 7 orders of magnitude below its cw intensity level (Fig. 1.1). As the demand for laser diodes grows, however, applications increasingly exist which require even lower levels of intensity noise. In coherent optical communications, for example, intensity noise in the local oscillator can increase the bit-error rate at the receiver.<sup>1</sup> The visibility of the fringe patterns from high precision interferometers and the sensitivity of spectroscopic techniques can also be augmented with a decrease in intensity noise.<sup>2,3</sup>

In this thesis we present intensity noise measurements for two different types of semiconductor lasers. Both of these lasers are presently employed in industrial and research projects worldwide. The fundamental quantum noise limit, predicted by the Heisenberg

uncertainty principle, is also determined experimentally. All laser noise measurements are compared with this fundamental limit.

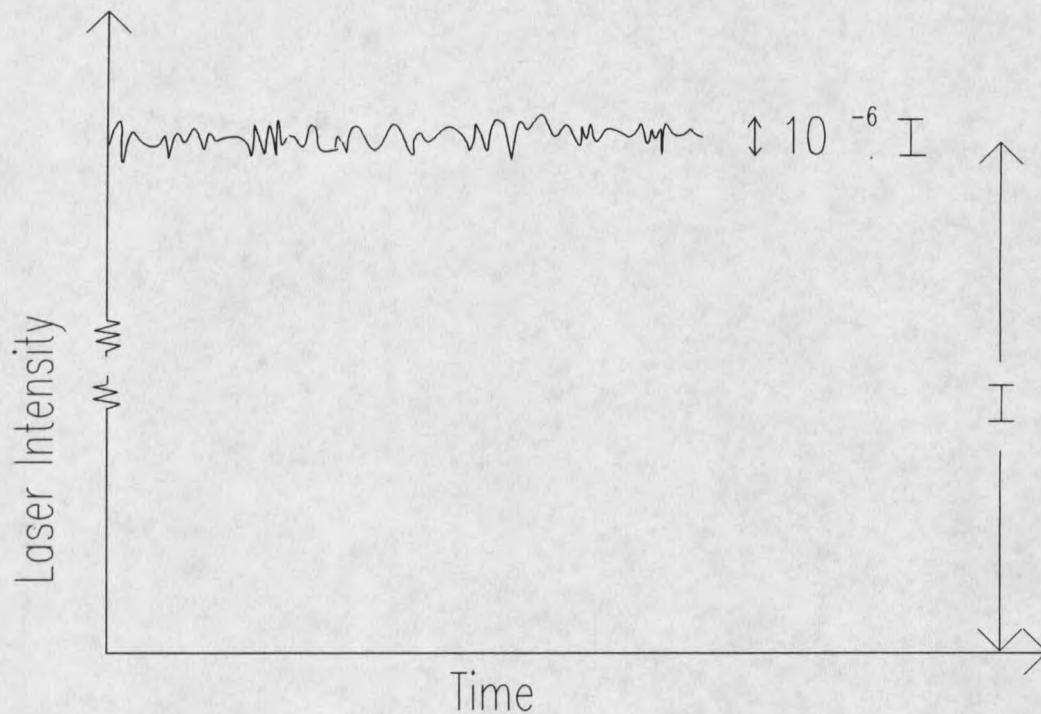


Figure 1.1. The optical intensity noise of a semiconductor laser is 5 to 7 orders of magnitude below the cw optical intensity level.

In addition, both a semiclassical and a fully quantum mechanical theoretical model of the intensity noise are used to model the experimental data. These models allow us to test not only to the accuracy of the theoretical formalisms, but also to gain insight into the sources of the intensity noise. In particular, the effects of quantum noise sources are investigated.

This thesis is organized into four chapters. In this first chapter we present background material to support and motivate this thesis project. A brief introduction to semiconductor

lasers is given and the main features of the intensity noise spectrum introduced. The standard quantum limit, with which we compare all our noise measurements, is discussed. Finally, a short review of previous work done on laser diode intensity noise in the frequency range 1-100 MHz is given, with comments on the relevance of this work.

Chapter 2 is devoted to both the semiclassical and the quantum theories of the intensity noise. The third and fourth chapters discuss experiments and results of intensity noise measurements. Chapter 3 deals with a free running laser diode (with no external optical feedback) and Chapter 4 with an external cavity laser diode (with external optical feedback). We end with a short conclusion in Chapter 5.

### Semiconductor Laser Basics

The simplest semiconductor laser is a forward biased p-n junction with cleaved ends (Fig. 1.2). The end surfaces act as partially reflecting mirrors and form the laser resonator. Electrons are pumped, by means of a constant dc current, into the conduction band, and "holes" are left behind in the valence band. When an electron in the conduction band decays back down to a hole in the valence band, via stimulated or spontaneous emission, a photon is generated. Typical dimensions of the laser are  $300 \times 200 \times 100 \text{ } (\mu\text{m})^3$ , much smaller than most other types of lasers; the lasing itself takes place right at the p-n junction, in an "active region" usually only 0.5 to 5  $\mu\text{m}$  thick. Most lasers today incorporate an additional layer of a slightly

different bandgap material between the p and n layers. As discussed in Chapter 3, this helps to confine the carriers to a smaller region.

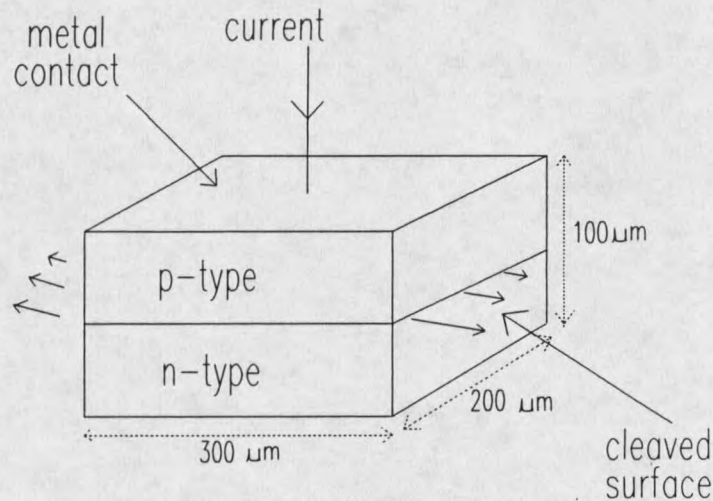


Figure 1.2. Semiconductor laser.

Because the conduction and valence bands are not discrete states, the gain profile of a semiconductor laser is exceptionally broad (Fig. 1.3). The gain profile shows the optical gain of the laser as a function of frequency (or wavelength). Due to the cavity resonances which occur when the length of the cavity  $L$  is an integral number of half wavelengths, the laser will prefer to operate at certain “longitudinal modes”. The longitudinal “side modes”, however, will never be completely suppressed. The doping level, laser structure, and pump level will all affect the magnitude of these side modes.

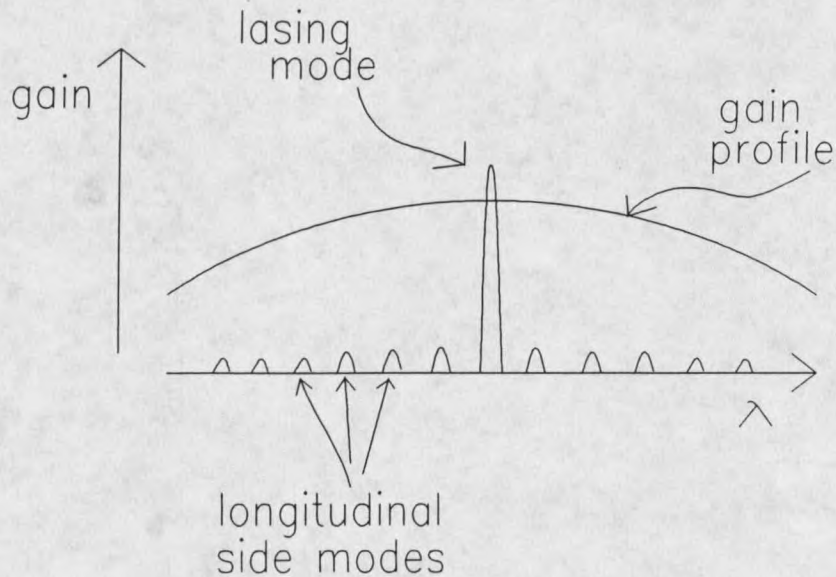


Figure 1.3. Longitudinal side modes exist due to the broad gain profile of the semiconductor laser, and the resonances of the laser cavity.

### Intensity Noise Spectrum

The main features of the intensity noise spectrum of a laser diode operating above threshold are shown in Fig. 1.4. Below 1 MHz the noise is dominated by flicker noise. This noise leads to a characteristic  $1/f$  fall-off (straight line on the log-log plot). Flicker noise is found in such diverse phenomena as the human heartbeat,<sup>4</sup> the relationship between intensity and pitch in music,<sup>4</sup> the current noise in a transistor,<sup>4</sup> and the intensity noise of a laser diode.<sup>5</sup> The origin of flicker noise is poorly understood, although chaos theory has made some progress.<sup>6</sup>

On the upper end of the spectrum, the noise is dominated by relaxation oscillations.<sup>7,8</sup>

In a semiconductor laser it takes significantly longer to pump carriers into the active region (or to create a population inversion) than it takes for photons, on average, to leave the laser cavity. These two rates, coupled with the nonlinear dynamics of the laser's exponential growth, can lead to turn on/turn off, behavior in the laser intensity. Thus a small fluctuation in either the carrier number or photon number will set up a "relaxation oscillation", which leads to a resonant condition with its peak frequency between 500 MHz and 10 GHz.

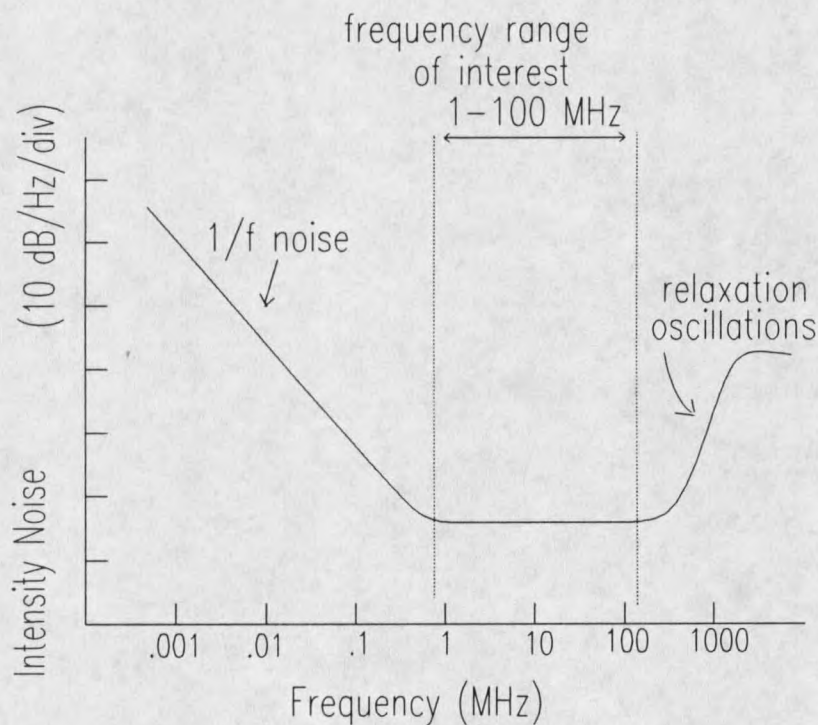


Figure 1.4. Intensity noise spectrum of a semiconductor laser.

The third regime (referred to as the low-frequency regime), and with which this thesis is concerned, is from 1 MHz to 100 MHz. Because the tail of the relaxation oscillations

becomes less prominent below 100 MHz and flicker noise occurs at frequencies below 1 MHz, two other noise sources can be studied. These are quantum and longitudinal side mode noise sources, which will dominate in the 1-100 MHz range at high pump levels. (The relaxation oscillation resonance frequency will shift to higher frequencies with an increase in the pump rate.)<sup>7</sup>

Although recent attention has been given to the mechanisms by which longitudinal side modes can increase the intensity noise of a semiconductor laser, significant uncertainty about this issue remains. In the case of mode partitioning, whereby the main mode and its side modes trade energy amongst themselves (if at any instant the intensity of the main mode decreases, the intensity of one or more side modes increases), the total intensity noise of the laser will either remain the same or increase. If the trading of energy is complete, such that the increase in power of one mode can exactly cancel the decrease in power of the other mode or modes, the total intensity noise will remain the same.<sup>9</sup> If on the other hand the trading of energy amongst the modes is not complete, or if there are frequency dependent losses within the cavity, the fluctuations of the individual modes in the output beam will not completely cancel one another. In this case the total intensity noise will increase.<sup>10,11</sup> Hole burning and other nonlinear gain mechanisms determine the degree of correlation between the modes.<sup>12</sup> A second mechanism by which side modes can add to the total intensity noise in this frequency range involves the shifting of side mode relaxation oscillations to lower frequencies.<sup>13</sup> This is facilitated by the coupling of the side modes to the main mode.

The intensity noise spectrum shown in Fig. 1.4 is for a laser pumped by an ideal, noise free controller (an ideal current or voltage source). Electromagnetic induction, however, from outside or inside the controller, can add electrical noise to the injection current. This in turn adds noise to the laser output. The controller must therefore be well shielded from the environment, and care must be taken to prevent “cross talk” between internal electronic components. Appendix A shows noise spectra for lasers being pumped by a well shielded battery, as well as by two non-ideal commercial controllers.

### The Shot Noise Limit (SNL)

In this thesis, experimental intensity noise measurements are compared with the “standard quantum limit” for intensity noise. The standard quantum limit is the noise associated with photon fluctuations which exhibit a Poisson distribution. The variance of the Poisson distribution gives the uncertainty in the number of photons ( $\Delta P$ ) as<sup>14</sup>

$$\Delta P = \sqrt{\bar{P}}, \quad (1.1)$$

where  $\bar{P}$  is the average number of photons detected in some measured time interval  $T$ . Particularly important is the coherent state of light, which in addition to possessing photon fluctuations with a Poisson distribution, also possesses photon and phase uncertainties which are at the minimum allowed by the uncertainty principle.

When photons with a Poissonian distribution impinge on a photodetector, they create an electrical current which we say is at the “shot noise limit” (SNL). The photon

statistics are transferred to the electrons, and therefore the electrons also have a Poissonian distribution. The variance of the shot noise of an electrical current can be found from Poissonian statistics and the definition of an electric current to be<sup>15</sup>

$$\Delta I = \sqrt{2qIB}, \quad (1.2)$$

with  $q$  the charge of an electron and  $B$  the bandwidth corresponding to  $\frac{1}{2T}$ . The shot noise limit given by Eq. (1.2) will be the standard to which all of our noise measurements will be compared.

### Recent Research

The intensity noise of semiconductor lasers has been studied theoretically since 1967,<sup>16</sup> and experimentally since 1977.<sup>17</sup> Because of the many parameters involved in the theory, and the difficulty in obtaining accurate values for these parameters, a relatively small portion of these studies compare theory and experiment. Our goal in this thesis was to obtain a detailed comparison of theory and experiment. To further this end, the parameters for the lasers discussed in this thesis are clearly derived or referenced. Then, the experimental intensity noise measurements made for the two different types of diode lasers are modeled, using both semiclassical and quantum theories.

The semiclassical Langevin laser theory discussed in this thesis was developed by Lax and Louisell in 1967,<sup>18,19</sup> and extended to the semiconductor laser by Henry in 1986.<sup>20</sup> The theory has mainly been used to analyze high frequency relaxation oscillations<sup>7</sup> as well as the

laser linewidth.<sup>21</sup> In this thesis the semiclassical theory is used to model intensity noise in the low-frequency regime (1-100 MHz); we find that the theory models our intensity noise measurements best when the side mode suppression is high, and relaxation oscillation noise is dominant. In this case the effects of mode partitioning, and quantum effects not modeled by the theory, are small.

The formulation of a fully quantum mechanical Langevin theory for the intensity noise of a semiconductor laser, was completed by Yamamoto *et al.* also in 1986.<sup>22</sup> This quantum formulation was spurred on by Yamamoto and his coworker's discovery of sub-shot noise light, generated from highly efficient laser diodes pumped by a low noise injection current.<sup>23</sup> To model this nonclassical light, the Langevin noise terms which are quantum in origin, were properly accounted for in this fully quantum mechanical theory. Since then, several groups, have generated sub-shot-noise (or squeezed) light using laser diodes,<sup>10,24,25</sup> and some have successfully modeled their results using the quantum theory.<sup>24,25</sup> By using the quantum and semiclassical theories to model our intensity noise measurements taken for two different types of lasers, we will establish even further the validity of all aspects of the quantum theory.

To generate photons with sub-Poissonian statistics, various types of laser diodes, in conjunction with different techniques (liquid nitrogen cooling, for example), have been utilized.<sup>10,23-25</sup> In contrast, we measure the intensity noise of an off-the-shelf diode laser, pumped by a commercial controller at room temperature. At injection currents of just twice threshold, the intensity noise is 5.5 dB above the SNL. The intensity noise of this same laser in a simple optical feedback configuration is also measured. The intensity noise is decreased from that of the free running laser (the solitary laser) by 10 dB just above threshold, and by 2.5 dB at

twice threshold. These results show that diode lasers, operated under the conditions employed for most practical applications, can also exhibit low levels of intensity noise in this low frequency regime.

## CHAPTER 2

## THE LANGEVIN RATE EQUATIONS

In this chapter, Langevin rate equations are used to develop both a semiclassical and fully quantum mechanical expression for the intensity noise of a semiconductor laser. In the semiclassical semiconductor laser theory the energy exchange between the carriers and the photons is discrete, and the electromagnetic field is described as a classical wave. The fully quantum mechanical semiconductor laser theory again describes the energy exchange as being discrete, but models the electromagnetic field quantum mechanically (as having both wave-like as well as particle-like characteristics). Differences in the derivation of both approaches are discussed, and the results quantitatively compared. In both cases the Langevin noise terms are at the heart of the laser intensity noise.

In order to simplify this theoretical analysis, the rate equations used here as a starting point for the derivation of the intensity noise, do not include an equation for the dipole moment of the laser medium. The equation for the dipole moment has been adiabatically eliminated,<sup>22,26</sup> this can be done because the dipole decay rate is much faster than both the photon and carrier decay rates. With the exception of our discussion of the noise processes in the laser, which requires proper consideration of dipole moment fluctuations, we will assume that the light interacts with the carriers instantaneously.

The theories presented here are for a laser with one longitudinal mode (as well as one spatial mode). As discussed in Chapter 1 of this thesis (Semiconductor Laser Basics), however, multiple longitudinal modes usually exist in a semiconductor laser. We will see in Chapters 3 and 4 that the effects of multiple modes lead to differences between our experimental results and theoretical predictions.

### Semiclassical Langevin Rate Equations

In a semiclassical description of a semiconductor laser, the light inside the laser cavity has a definite energy. In this section, that energy will be expressed as

$$E = P \cdot \hbar\omega_L, \quad (2.1)$$

where  $P$  represents the number of photons inside the laser cavity and  $\hbar\omega_L$  is the energy of each photon. Note that although the exchange of energy between the carriers and the light inside the cavity is quantized,  $P$  is a continuous quantity in this semiclassical theory.  $P$  is used as a convenient measure of the light inside the cavity only, and does not imply that the light is composed of discrete units. This would require the full quantum theory discussed in the next section.

The single mode rate equations for the number of photons  $P$  and the number of carriers  $N$  inside the laser cavity are<sup>27</sup>

$$\dot{P} = \left(G - \frac{1}{\tau_p}\right)P + R_{sp} + F_p(t) \quad (2.2a)$$

$$\dot{N} = \frac{I}{q} - \frac{N}{\tau_{sp}} - GP + F_N(t). \quad (2.2b)$$

In Eq. (2.2a) the term  $GP$  represents the exponential growth rate of the photons due to gain,  $-\frac{P}{\tau_p}$  the photon loss rate from the laser cavity,  $R_{sp}$  the rate of spontaneous emission into the lasing mode, and  $F_p(t)$  the random fluctuations in these three processes. The rate equation for  $N$  includes terms accounting for the rate at which carriers are pumped into the active region  $I/q$ , the rate of spontaneous carrier recombination  $-\frac{N}{\tau_{sp}}$ , the rate of stimulated photon emission  $-GP$ , and the fluctuations in these processes  $F_N(t)$ .

More specifically  $\tau_{sp}$  is the spontaneous recombination lifetime, and represents the average time an electron remains in the conduction band before spontaneously decaying, either radiatively or nonradiatively, back down to the valence band. The photon life time  $\tau_p$  accounts for the lifetimes  $\tau_i$  and  $\tau_e$ , associated with the internal and external losses, such that

$$\frac{1}{\tau_p} = \frac{1}{\tau_i} + \frac{1}{\tau_e}. \quad (2.3)$$

Internal losses include carrier scattering at p-n junctions and carrier absorption, while the external losses comprise the laser output. The current into the active region is denoted by  $I$  and the charge of an electron by  $q$ .

$G$ , the gain, is expressed as

$$G = \alpha(N - N_o). \quad (2.4)$$

In this expression  $\alpha$  is the gain coefficient and  $N_0$  the number of carriers needed to achieve transparency (population inversion). A self saturation term (proportional to  $P$ ) is not included in  $G$ ; its contribution to the intensity noise is insignificant in our case.

The Langevin noise sources  $F_P(t)$  and  $F_N(t)$  account for the random fluctuations in  $P$  and  $N$ . They satisfy the conditions<sup>28,29</sup>

$$\langle F_i(t) \rangle = 0 \quad (2.5a)$$

$$\langle F_i(t)F_j(t') \rangle = 2D_{ij}\delta(t-t'). \quad (2.5b)$$

Equation (2.5a) shows that the noise processes are indeed random, as they average to zero over time. The delta function in Eq. (2.5b) implies that the fluctuations are Markovian; that is, the fluctuations are completely uncorrelated in time. The  $D_{ij}$ 's are the diffusion coefficients, and give the magnitude of the fluctuations.

In the semiclassical model, the steady processes affecting  $P$  and  $N$  (given by the terms in the rate equations) are modeled as discrete random events. Because random events have a Poissonian distribution, the  $D_{ij}$ 's account for shot noise level fluctuations of these processes (see The Shot Noise Limit in Ch.1 of this thesis). Found by classical statistical arguments or by applying the fluctuation-dissipation theorem to the Langevin rate equations, the diffusion coefficients are<sup>27</sup>

$$D_{PP} = R_{sp}P \quad (2.6a)$$

$$D_{PN} = -R_{sp}P \quad (2.6b)$$

$$D_{NN} = R_{sp}P + \frac{N}{\tau_{sp}} \quad (2.6c)$$

$D_{PP}$  and  $D_{NN}$  represent the magnitude of the random fluctuations for all steady state processes affecting  $P$  and  $N$ . The magnitude of the fluctuations in  $P$ , which are anticorrelated with fluctuations in  $N$ , are represented by  $D_{PN}$ . Appendix B shows the diffusion terms rewritten in terms of these processes.

To solve the nonlinear coupled rate equations for  $P$  and  $N$ , a small-signal approximation is used for the variation from steady state. We let  $P$ ,  $N$ , and  $G$  vary from their steady state values by amounts  $\delta P$ ,  $\delta N$ , and  $\delta G$ ; where  $\delta P$ ,  $\delta N$ ,  $\delta G \ll P$ ,  $N$ ,  $G$ . Keeping only linear terms in  $\delta P$ ,  $\delta N$ ,  $\delta G$  (final results show  $\delta P/P \ll 10^{-7}$ ), the resulting equations are

$$\delta \dot{P} = -\Gamma_P \delta P + \alpha P \delta N + F_P(t). \quad (2.7a)$$

$$\delta \dot{N} = -\Gamma_N \delta N - G \delta P + F_N(t). \quad (2.7b)$$

In obtaining Eq. (2.7a) we let  $G = \alpha \delta N$  from Eq. (2.4), and used the steady state form of Eq (2.2a) to solve for  $(G - \frac{1}{\tau_p})$ . The photon and carrier fluctuation decay rates,  $\Gamma_P$  and  $\Gamma_N$ , are defined as<sup>27</sup>

$$\Gamma_P = \frac{R_{sp}}{P} \quad (2.8a)$$

$$\Gamma_N = \frac{1}{\tau_{sp}} + \alpha P. \quad (2.8b)$$

(Recall that these are the two different decay rates for  $P$  and  $N$  which are responsible for the relaxation oscillations discussed in Chapter 1.) Applying the fourier transform

$$\delta P(\omega) = \int_{-\infty}^{\infty} \delta P(t) e^{-i\omega t} dt \quad (2.9)$$

to Eqs. (2.7a) and (2.7b) (the intensity noise will be measured per unit bandwidth), gives

$$(\Gamma_P + i\omega)\delta P(\omega) - \alpha P \delta N(\omega) = F_P(\omega) \quad (2.10a)$$

$$(\Gamma_N + i\omega)\delta N(\omega) + G\delta P(\omega) = F_N(\omega). \quad (2.10b)$$

(Note that in order to obtain the fourier transform of  $\delta \dot{P}$  and  $\delta \dot{N}$  in Eqs. (2.7a) and (2.7b),

we used for example the relationship  $\delta P(t) = \int_{-\infty}^{\infty} \delta P(\omega) e^{i\omega t} d\omega$ , so that  $\delta \dot{P} = i\omega \delta P$ .) For

frequencies less than 100 MHz and injection currents larger than threshold, terms in  $\omega$  can be dropped: they contribute less than 2% to the final result.

The spectral noise density for the photons inside the cavity is defined as<sup>30</sup>

$$S_P(\omega) = \lim_{T \rightarrow \infty} \frac{2}{T} \langle \delta P(\omega, T) \delta P(\omega, T) \rangle. \quad (2.11a)$$

The noise density is measured only at positive frequencies, and therefore Eq. (2.11a) represents the single-sided noise density. Solving for  $S_P(\omega)$  using Eqs. (2.10a) and (2.10b)

we find

$$S_P(\omega) = \lim_{T \rightarrow \infty} 2 \left[ \frac{\Gamma_N^2 \langle |\delta F_P(\omega, T)|^2 \rangle + \alpha^2 P^2 \langle |\delta F_N(\omega, T)|^2 \rangle}{(\Gamma_P \Gamma_N + G\alpha P)^2} \right. \\ \left. \frac{2\alpha P \Gamma_N \langle |F_P(\omega, T) F_N(\omega, T)| \rangle}{(\Gamma_P \Gamma_N + G\alpha P)^2} \right] \quad (2.11b)$$

Using the Wiener-Khinchin theorem we can write<sup>30</sup>

$$\lim_{T \rightarrow \infty} \langle \delta F_i(\omega, T) \delta F_j(\omega, T) \rangle = \int_{-\infty}^{\infty} \langle \delta F_i(t) \delta F_j(t + \tau) \rangle e^{-i\omega\tau} d\tau. \quad (2.11c)$$

The delta functions in the Langevin correlation functions, Eq. (2.5b), collapse the integral on the right side of Eq. (2.11c), and we find

$$S_p(\omega) = \frac{2[\Gamma_N^2 D_{PP} + \alpha^2 P^2 D_{NN} + 2\alpha P \Gamma_N D_{PN}]}{(\Gamma_P \Gamma_N + G\alpha P)^2}. \quad (2.12)$$

This is our expression for the spectral photon noise of the photons inside the laser cavity.

Next, we find the spectral noise density for the light intensity outside the laser cavity. The spectral noise density for the light outside the laser cavity,  $S_o(\omega)$ , in units of  $W^2/Hz$ , can be written in terms of  $S_p(\omega)$  as

$$S_o(\omega) = \left(\frac{1}{\tau_e} \hbar\omega_L\right)^2 S_p(\omega). \quad (2.13)$$

Here,  $\hbar\omega_L$  is the energy of each photon. Finally, to normalize  $S_o(\omega)$  to the SNL, we note that the rate of photons emerging from the laser which are associated with the shot noise is  $\left(\frac{2P}{\tau_e}\right)^{1/2}$  with units of  $Hz^{1/2}$ . (This can be found from Eq. (1.1), letting  $T=1/2B$  with  $B=1$

Hz). The shot noise density,  $S_{SNL}$ , in units of  $W^2/Hz$ , is related to  $P$  by

$$S_{SNL} = \frac{2(\hbar\omega_L)^2 P}{\tau_e}. \quad (2.14)$$

Substituting  $S_p(\omega)$  from Eq. (2.12) into Eq. (2.13), and dividing by  $S_{SNL}$  from Eq. (2.14), we arrive at an expression for the output spectral noise density normalized to the shot noise density

$$\frac{S_o(\omega)}{S_{SNL}} = \frac{2}{\tau_e} \left[ \frac{\left( \frac{1}{\tau_{sp}} + \alpha P \right)^2 D_{PP} + \alpha^2 P^2 D_{NN} + 2\alpha P \left( \frac{1}{\tau_{sp}} + \alpha P \right) D_{PN}}{2G^2 \alpha^2 P^3} \right], \quad (2.15)$$

where only the dominant term in the denominator has been kept.

In our experiment and in many applications, the laser's optical power is converted to an electrical signal via a photodiode and rf spectrum analyzer. The mathematical steps taken in Eqs. (2.12)-(2.15) are equivalent to these experimental operations. In the rest of this thesis,  $S_o(\omega)$  will be referred to as the intensity noise of the laser and  $S_o(\omega)/S_{SNL}$  as the intensity noise normalized to the SNL.

### Quantum Mechanical Rate Equations

The quantum mechanical Langevin rate equations used to derive an expression for the intensity noise of a semiconductor laser, give the time rate of change of the electric field annihilation and carrier number operators,  $\hat{A}$  and  $\hat{N}$ . (The electric field operator  $\hat{A}$  is used in this case instead of the photon number operator  $\hat{A}^\dagger \hat{A}$ , in order to appropriately couple noise terms as discussed below). The Heisenberg representation of the laser system is thereby employed, where the operators evolve in time and the wavefunction of the system remains constant in time.

The rate equations for the electric field and carrier number operators  $\hat{A}$  and  $\hat{N}$  are<sup>22</sup>

$$\frac{d\hat{A}}{dt} = -\frac{1}{2} \left[ \frac{1}{\tau_p} + 2j(\omega - \omega_o) - \frac{\omega}{\mu^2} (\hat{\chi}_i - j\hat{\chi}_r) \right] \hat{A} + \hat{M}(t) + \hat{m}(t) + \hat{f}(t) \quad (2.16a)$$

$$\frac{d\hat{N}}{dt} = \frac{I}{q} - \frac{\hat{N}}{\tau_{sp}} - \hat{G}\hat{P} + \hat{\Gamma}(t) + \hat{\Gamma}_I(t) + \hat{\Gamma}_{sp}(t). \quad (2.16b)$$

In the rate equation for the field annihilation operator  $\hat{A}$ , the first term  $\frac{1}{\tau_p}$  accounts for internal and external (output) photon losses. These losses are the same as those described in the semiclassical theory by Eq. (2.3). The laser oscillation frequency and the laser atomic resonance frequencies are given by  $\omega$  and  $\omega_o$ . The second term therefore denotes the change in phase of the electric field due to the "detuning" ( $\omega - \omega_o$ ). In the third term, imaginary and real parts of the susceptibility operator, operators representing the gain and the dispersion of the system respectively, are given by  $\hat{\chi}_i$  and  $\hat{\chi}_r$ , and the index of refraction of the laser medium by  $\mu$ . The Langevin noise operators  $\hat{M}(t)$ ,  $\hat{m}(t)$ , and  $\hat{f}(t)$ , represent the fluctuations in the above three processes involving the electric field.

The first three terms in the rate equation for the operator  $\hat{N}$  represent the same processes as those in the semiclassical rate equation for the number of carriers  $N$ . The first term  $\frac{I}{q}$  gives the rate of carriers injected into the active region by the pump, the second term  $\frac{\hat{N}}{\tau_{sp}}$  the rate of spontaneous carrier recombination, and the third term  $\hat{G}\hat{P}$  the rate of carriers lost due to stimulated emission. The Langevin noise terms are not grouped together as one term as in the semiclassical case ( $F_N(t)$  in Eq. (2.2b)), but are separated

into 3 noise operators  $\hat{\Gamma}(t)$ ,  $\hat{\Gamma}_I(t)$ , and  $\hat{\Gamma}_{sp}(t)$ . These terms represent the fluctuations of the above three processes involving the carriers.

The six noise operators satisfy similar conditions as those of the corresponding semiclassical Langevin noise terms. The expectation value of each operator averages to zero over time. The correlation functions for the operators are delta correlated in time, and have the general form<sup>22,29</sup>

$$\langle \hat{O}_i(t) \hat{O}_j(t') \rangle = 2D_{O_i O_j} \delta(t - t') \quad (2.17)$$

where  $\hat{O}_i$  and  $\hat{O}_j$  are two Langevin noise operators.

The reservoir theory of a semiconductor laser is used to model the noise processes of the laser (Fig. 2.1).<sup>26,29</sup> In this theory discrete loss or gain processes to or from systems of interest are modeled by "system-reservoir" interactions. For example, as shown in Fig. 2.1, the internal field of the laser experiences loss through the output ports of the laser. There are fluctuations in the loss rate due to the discrete nature of the photons. These fluctuations are represented by the Langevin noise operator  $\hat{f}$  in the rate equations in Eq. (2.16a), and describe the internal field system interacting with the external loss reservoir. As another example, the Langevin noise operator  $\hat{\Gamma}$  represents the interaction between the reservoir associated with atomic collisions and the carrier system. (The dipole moment system has been adiabatically eliminated as discussed at the beginning of this chapter.) The other noise operators model system reservoirs in a similar manner.

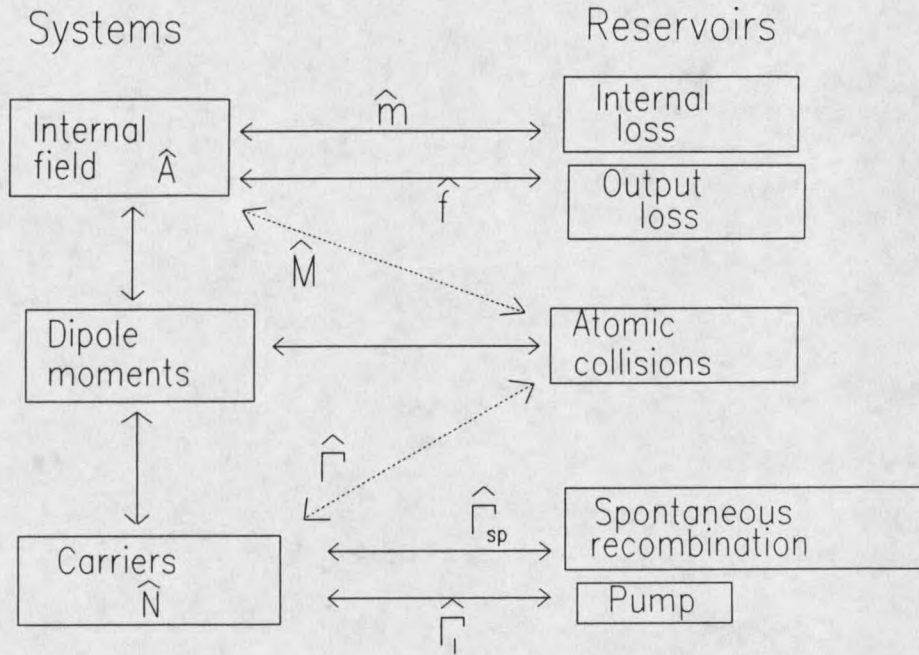


Figure 2.1. The reservoir model for the noise processes of the semiconductor laser.

In the rate equation (2.16a),  $\hat{m}$  and  $\hat{f}$  represent fluctuations due to the interaction between the internal field system and the internal and output loss reservoirs. The operators  $\hat{\Gamma}_{sp}$  and  $\hat{\Gamma}_i$  in Eq. (2.16b) represent fluctuations due to the interactions between the carrier system and the reservoirs associated with spontaneous recombination and the pump. The magnitudes of all these noise processes can be determined from the fluctuation-dissipation theorem. The diffusion coefficients in Eq. (2.17) for the operators,  $\hat{m}$ ,  $\hat{f}$ , and  $\hat{\Gamma}_{sp}$  are then given by<sup>22</sup>

$$D_{ff} = \frac{1}{8\tau_e} \quad (2.18a)$$

$$D_{mm} = \frac{1}{8\tau_i} \quad (2.18b)$$

$$D_{\Gamma_p \Gamma_p} = \frac{\langle \hat{N} \rangle}{2\tau_{sp}} \quad (2.18c)$$

The diffusion coefficient for the pump noise ranges from  $D_{\Gamma_r \Gamma_r} = 0$  to  $D_{\Gamma_r \Gamma_r} = \frac{\langle I \rangle}{2q}$ ,

and will be discussed in a separate section below.

The noise operators  $\hat{M}$  and  $\hat{\Gamma}$  represent the fluctuations of the internal field and carrier systems with the reservoir associated with atomic collisions. These loss (or gain) processes occur via the dipole moment system as shown in Fig. 2.1. Therefore atomic collisions in the laser medium, which cause dipole dephasing, are the noise source of the reservoir-system interactions represented by  $\hat{M}$  and  $\hat{\Gamma}$ . The diffusion coefficients for the correlation function of these operators are given by<sup>22</sup>

$$D_{MM} = \frac{1}{8} \alpha \left[ \langle \hat{N} \rangle + N_o \right] \quad (2.19a)$$

$$D_{\Gamma\Gamma} = \frac{1}{2} \alpha \left[ \langle \hat{N} \rangle + N_o \right] \langle \hat{P} \rangle. \quad (2.19b)$$

As illustrated by Fig. 2.1, each dipole moment fluctuation affects both the photon field and the carriers. Also, for each carrier lost from the carrier system, by means of the dipole moment system, a photon is added to the internal field system. This means that the noise

operators  $\hat{M}$  and  $\hat{\Gamma}$  are correlated. The diffusion coefficient for the correlation of  $\hat{M}$  and  $\hat{\Gamma}$  is given by<sup>22</sup>

$$D_{MT} = -\frac{1}{4}\alpha\left[\langle\hat{N}\rangle + N_o\right]\langle\hat{A}\rangle. \quad (2.19c)$$

Due to the fluctuations in the output coupling represented by the noise operator  $\hat{f}$ , the output field of the laser is not directly proportional to the internal field of the laser. Figure 2.2 shows the relationship between the output field flux operator  $\hat{r}$  and the internal field operator  $\hat{A}$ .<sup>22,31</sup> The fluctuations represented by the external field output coupling operator  $\hat{f}_e$ , which is related to the internal field output coupling noise operator  $\hat{f}$  by

$$\hat{f} = \left(\frac{1}{\tau_{sp}}\right)^{\frac{1}{2}} \hat{f}_e, \quad (2.20)$$

are added to the internal field such that

$$\hat{r} = -\hat{f}_e + \left(\frac{1}{\tau_{sp}}\right)^{\frac{1}{2}} \hat{A}. \quad (2.21)$$

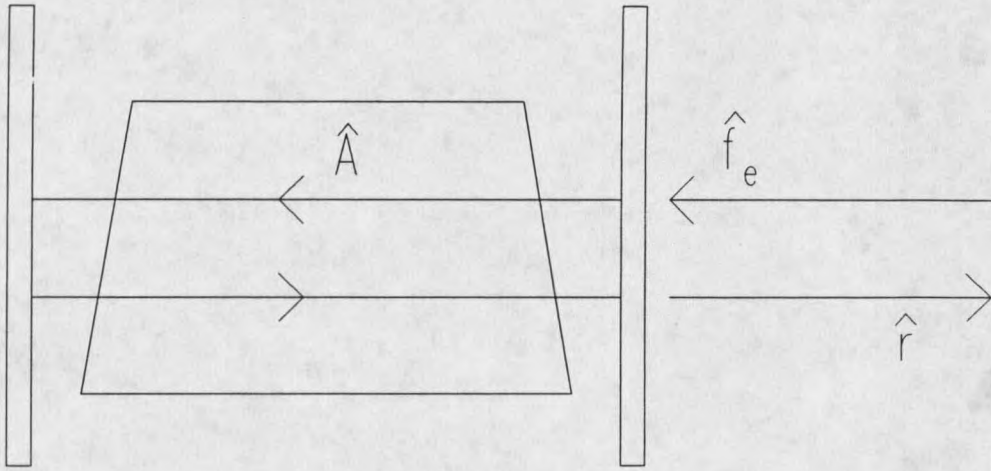


Figure 2.2. Theoretical laser model showing the operators for the internal field  $\hat{A}$ , the external vacuum field flux  $\hat{f}_e$ , and the external output field flux  $\hat{r}$ .

The derivation for the intensity noise normalized to the SNL,  $\frac{S_o(\omega)}{S_{SNL}}$ , is similar to that for the semiclassical case and given in reference [22]. The two main differences in the derivations are the use of the electric field operator in the quantum derivation (instead of an operator for the photon number) and the incorporation of the output coupling noise in obtaining the output field from the internal field.

From the derivation outlined in reference [22], we find the final result for the intensity noise normalized to the SNL to be

$$\begin{aligned}
\frac{S_o(\omega)}{S_{SNL}} = \frac{2}{\tau_e} & \left[ \frac{4P\left(\frac{1}{\tau_{sp}} + \alpha P\right)^2 (D_{MM} + D_{mm} + D_{ff})}{2G^2 \alpha^2 P^3} \right. \\
& \frac{4P\left(2\tau_e \alpha GP\left(\frac{1}{\tau_{sp}} + \alpha P\right) - \tau_e^2 G^2 \alpha^2 P^2\right) D_{ff}}{2G^2 \alpha^2 P^3} \\
& \left. + \frac{\alpha^2 P^2 (D_{\Gamma\Gamma} + D_{\Gamma\Gamma_i} + D_{\Gamma_{sp}\Gamma_{sp}})}{2G^2 \alpha^2 P^3} + \frac{4\alpha P \langle \hat{A} \rangle \left(\frac{1}{\tau_{sp}} + \alpha P\right) D_{M\Gamma}}{2G^2 \alpha^2 P^3} \right] \quad (2.22)
\end{aligned}$$

with the diffusion coefficients given by Eqs.(2.18a-c) and (2.19a-c). The magnitude of the correlation function for the injection current  $D_{\Gamma_i\Gamma_i}$  is discussed in the next section.

Equations (2.15) and (2.22) are the semiclassical and quantum versions of the quantity we measure experimentally,  $\frac{S_o(\omega)}{S_{SNL}}$ , the intensity noise normalized to the SNL.

Using Appendix C, in which we have rewritten the semiclassical Langevin diffusion coefficients in more intuitive forms, one can compare Eqs. (2.15) and (2.22). With just two exceptions, all terms in the semiclassical expression have a corresponding quantum mechanical analogue.

The first term in Eq. (2.22), which contains the field diffusion coefficients, corresponds to the first term in Eq. (2.15) exactly. (We replace  $D_{PP}$  in Eq. (2.15) with the expression given by Eq. (C.5)). Term two in Eq. (2.22) is due to the external output

coupling noise operator  $-\hat{f}_c$ , and does not have a corresponding term in Eq. (2.15). The semiclassical theory does not include an external output coupling noise term, as the internal photon number fluctuations are directly proportional to the external photon number fluctuations. The third term in Eq. (2.22), which contains the carrier number diffusion coefficients, corresponds to the second term in Eq. (2.15) exactly.

Although the fourth term in Eq. (2.22) containing the cross correlation diffusion coefficient corresponds to the third term in Eq. (2.15), they are not exactly equal to one another. This is because in the quantum theory the photon system is coupled to the carrier system only via the reservoir associated with atomic collisions ( $\langle \hat{M}(t)\hat{\Gamma}(t') \rangle \neq 0$ ). In the semiclassical theory however, the photons and carriers are coupled not only by atomic collisions, but also by the external and internal photon losses. The latter coupling process means that for every photon lost through the output port of the laser or internally, a carrier will recombine and create a photon. Thus there is an "extra" term in the semiclassical cross correlation diffusion coefficient proportional to  $-\frac{P}{\tau_p}$  (Eq. C.11), which is not present in the quantum theory.

### Pump Noise

The noise operator  $\hat{\Gamma}_I$  represents the noise of the pump reservoir interacting with the carrier system. Fluctuations in the diode impedance are the source of this noise.<sup>22,32</sup>

If the injection current is generated by a "voltage source", the injection current electrons will have a Poissonian distribution in time, and the pump noise operator  $\hat{\Gamma}_I$  will add the shot noise of the pump to the carrier system. This configuration is depicted schematically in Fig. 2.3. A voltage source has a small source resistance,  $R_s \ll R_L$ , and fluctuations in the diode impedance will be transferred to the electrons in the injection current ( $V=I(R_s+R_L)$ ). The interaction of the laser, and a pump with shot noise statistics, is given by the diffusion coefficient of the pump noise operator  $\hat{\Gamma}_I$ , as

$$D_{r,r_i} = \frac{\langle I \rangle}{2q}. \quad (2.23a)$$

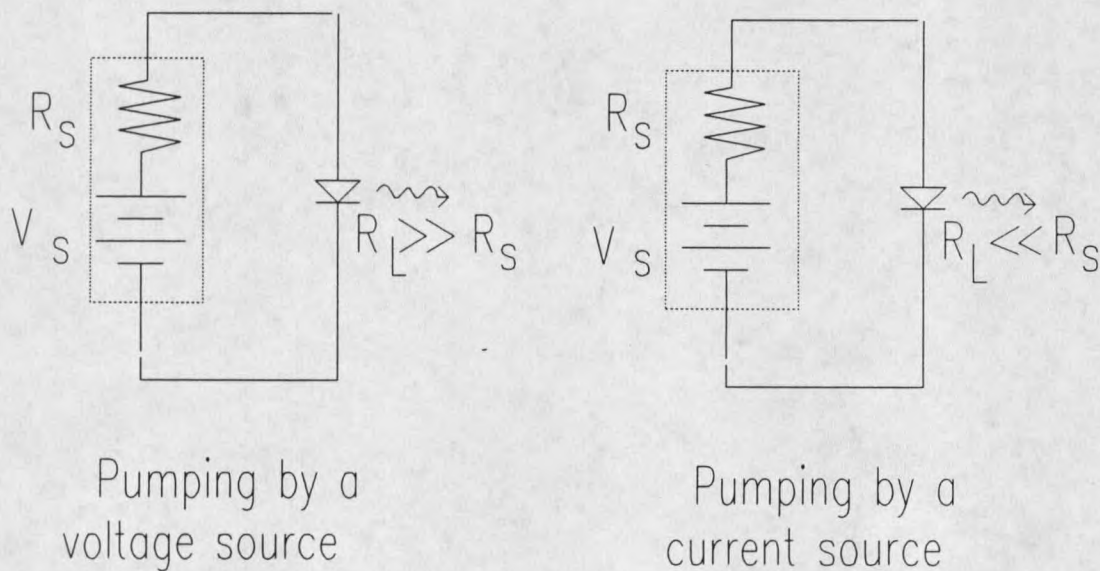


Figure 2.3. Schematic of a diode laser pumped by a constant voltage and constant current sources.

If the injection current is generated by a "current source", the pump noise operator will not add any noise to the carrier system. As shown in Fig 2.3  $R_L \ll R_s$  for a current source and fluctuations in the diode resistance will have a negligible effect on the current. Then diode impedance fluctuations will not dominate over the mutual coulombic repulsion of the electrons, and the electrons will arrive at the laser at essentially regular time intervals. The dominant noise source in this case is thermal noise, which is more than 2 orders of magnitude smaller than the calculated shot noise for the pump  $\frac{4k_B T B}{R} \ll 2q\langle I \rangle B$ , thus the diffusion coefficient can effectively be set to zero,

$$\hat{D}_{\Gamma, \Gamma'} \cong 0. \quad (2.23b)$$

The quantum mechanical theoretical intensity noise  $\frac{S_o(\omega)}{S_{SNL}}$  given by Eq. (2.22), both with and without pump noise, is plotted in Fig. 2.4. Appendix B gives values for the parameters used in the theory; they are the same as those determined for the diode laser discussed in Chapter 3. When the magnitude of the pump noise is given by Eq. (2.23a) (voltage source), the intensity noise of the laser approaches the SNL for high pump rates; the statistics of the electrons are transferred to the photons. When there is no pump noise (current source), the intensity noise drops below the SNL at high pump rates.

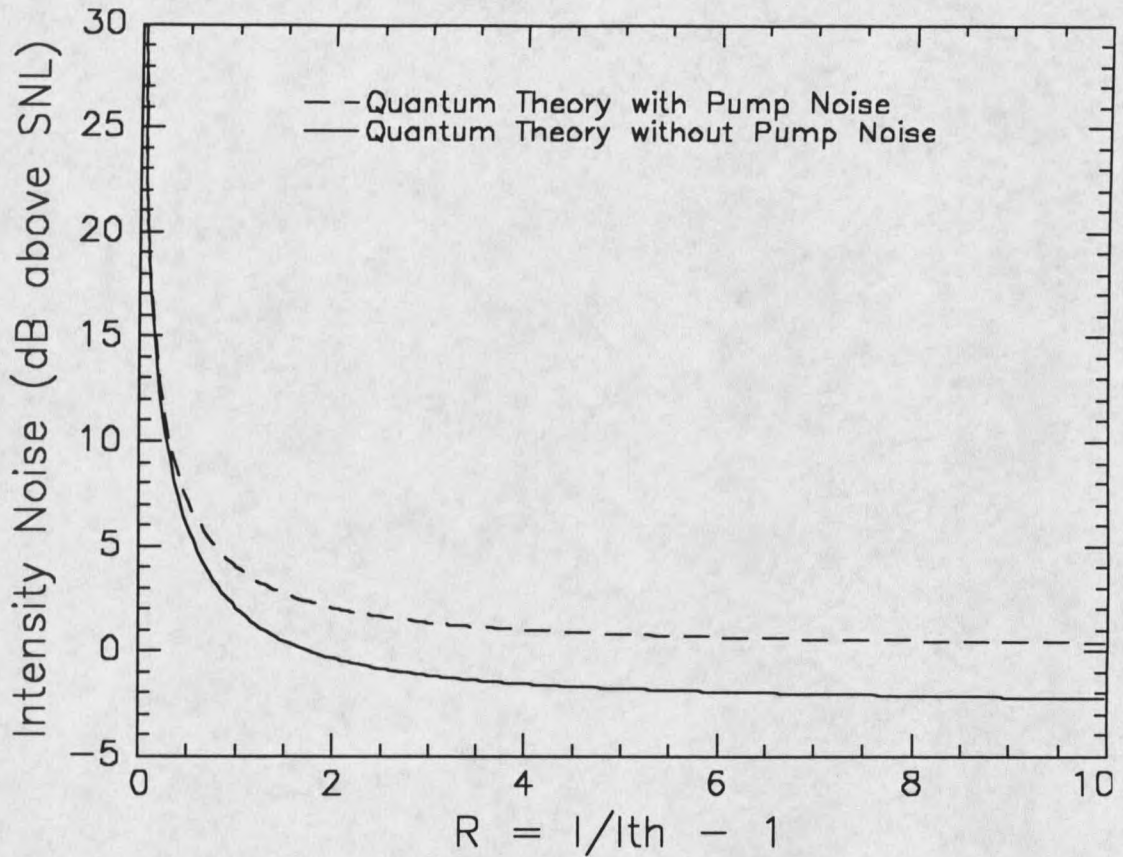


Figure 2.4. The quantum mechanical theoretical intensity noise for the cases when the pump noise is zero and when it is at the SNL.  $R$  is the normalized threshold injection current;  $I$  is the injection current and  $I_{th}$  the threshold injection current.

#### Quantitative Comparison

The intensity noise as a function of injection current for the semiclassical and quantum theories are shown Fig. 2.5. The two single mode theories agree at low injection currents where relaxation oscillations dominate (see Intensity Noise Spectrum in Chapter 1 of this thesis). The two theories begin to deviate at injection currents near 1.5 times threshold ( $R=0.5$ ), and the semiclassical theory drops below the SNL at 1.7 times

threshold ( $R=0.7$ ). The low level of intensity noise predicted by semiclassical theory at higher pump rates is due in large part to the inclusion of  $-\frac{P}{\tau_p}$  in the cross correlation diffusion coefficient (see the last paragraph before the section Pump noise above, and Eq. (C.11)).

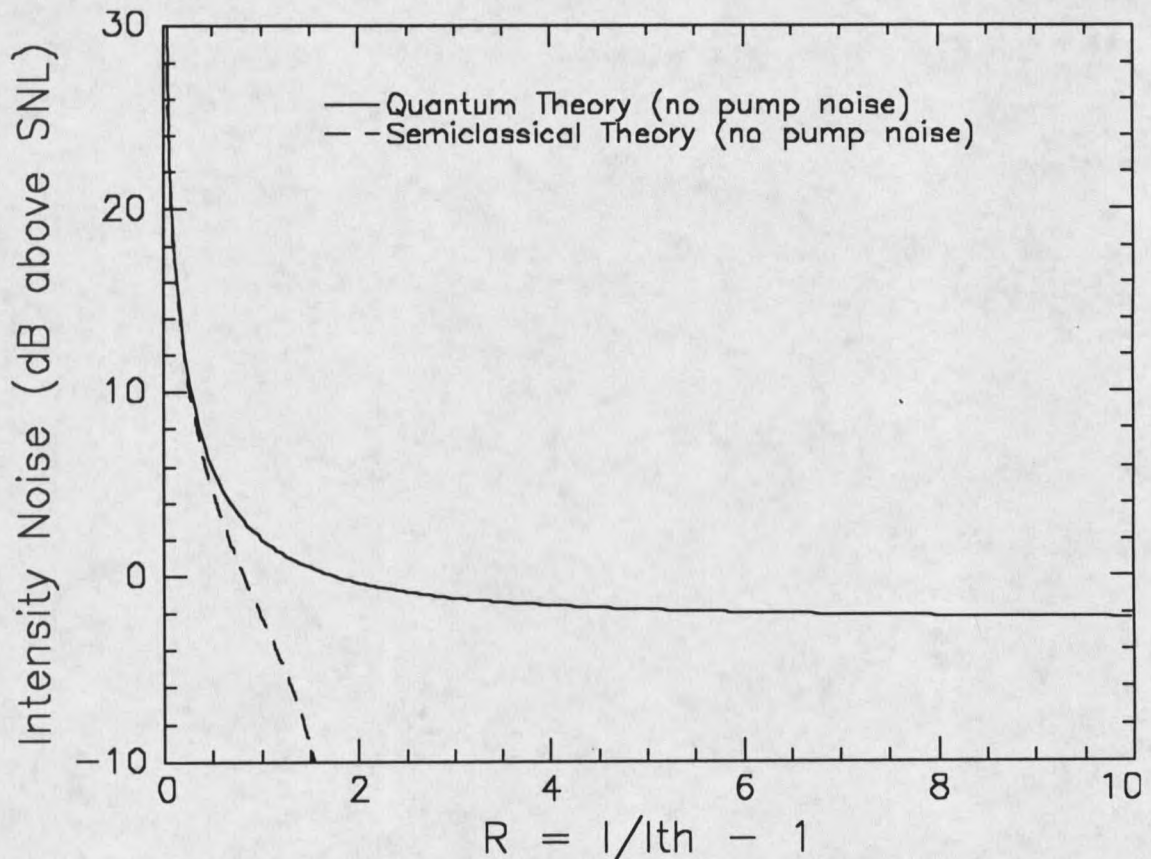


Figure 2.5. The theoretical quantum (solid line) and semiclassical (dashed line) intensity noise as a function of injection current. Neither theory includes pump noise.

## CHAPTER 3

## SEMICONDUCTOR LASER

In this chapter the experimental setup and procedure for intensity noise measurements of a free running laser diode are discussed. "Free running" here means that the laser cavity has not been altered by optical elements placed external to the diode (as will be the case in Chapter 4). The experimental results are presented and modeled with both the semiclassical and quantum mechanical theoretical expressions from Chapter 2.

Laser Diode

The laser discussed in this chapter is Sharp's model LTO25MDO which operates at a nominal power of 30 mW. The active region, the region of the diode in which the carriers and light are concentrated, is GaAlAs, and the band gap of this material gives a lasing wavelength of 788 nm. A highly reflective coating has been put on the back surface of the laser (97% reflective) and an antireflective (AR) coating on the front surface (0.65% reflective nonideal AR coating). Thus almost all of the light is emitted from the front surface.

These lasers have a double buried heterostructure as shown in Fig. 3.1. This means that the active region is surrounded on all sides by slightly different semiconductor materials (in

this case GaAs with different aluminum dopant levels). The layers above and below the active region have a larger bandgap than that of the active region which helps to confine the carriers. Additionally, the material to the sides of the active region has a higher index of refraction than that of the active region, producing a waveguiding effect that helps to confine the light. Therefore, a double buried heterostructure keeps a high concentration of both carriers and light in the active region, thus improving the efficiency of the laser.

The temperature of the laser was maintained at  $20.0^{\circ}\text{C} \pm 0.1^{\circ}\text{C}$  using an ILX model LDT-5412 temperature controller. The current was ramped from just above threshold to twice threshold using an ILX model LDX-3620 low noise current controller.

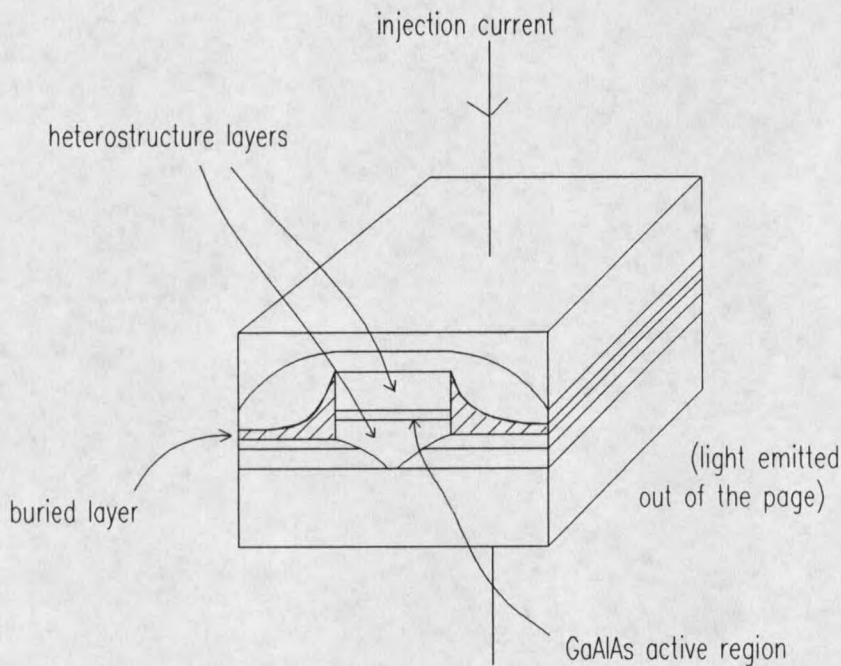


Figure 3.1. The double buried heterostructure semiconductor laser used in this first intensity noise experiment.

### Laser Intensity Noise Measurements

Figure 3.2 shows the experimental setup for measuring the intensity noise of the laser diode. A Hamamatsu model S3994 photodiode was used to detect the laser beam. Although this detector has only a 3 dB bandwidth of 30 MHz, it has a high quantum efficiency of 92% at 788 nm as well as a large 1 cm x 1 cm active region for excellent saturation properties. A high quantum efficiency means that photons incident on the detector have a high probability of generating an electron for the output current.

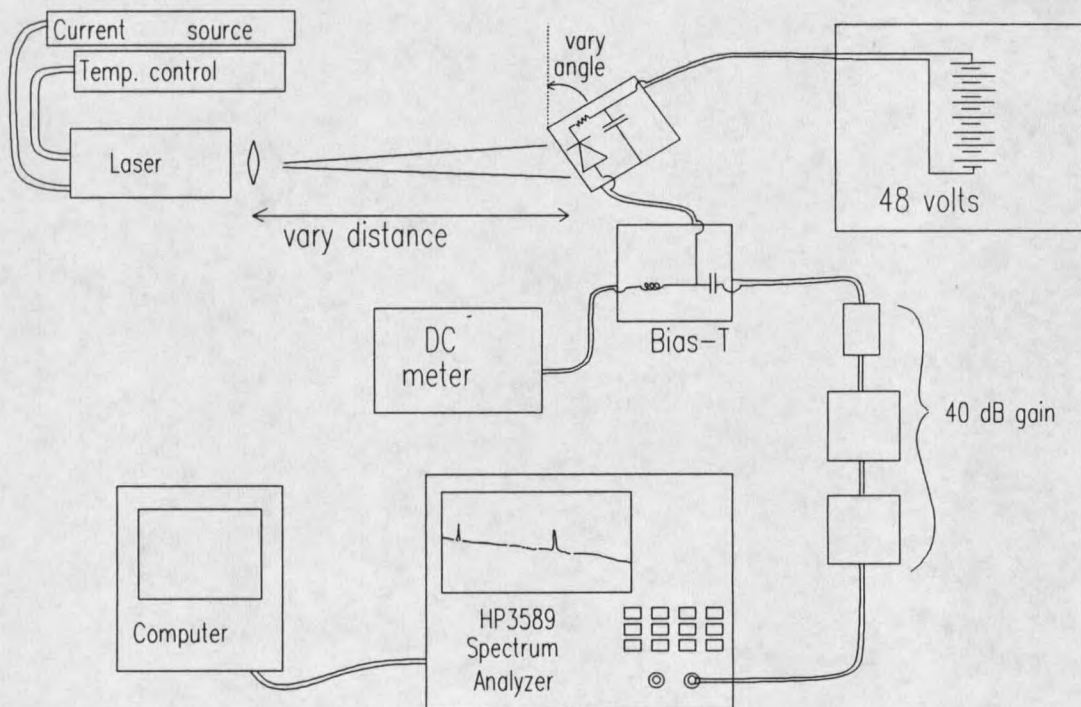


Figure 3.2. Experimental setup used to measure the laser intensity noise at 25 MHz.

The photodiode was followed by a bias-T which separated the ac and the dc parts of the electrical signal. The ac signal then passed through three low noise electronic amplifiers (one Anzac model AM-117 with a gain of 8 dB and two Anzac models AM-112 with gains of 16 dB), and into an HP3589A rf spectrum analyzer. The noise floor of the three cascaded amplifiers was -126 dBm/Hz while that of the spectrum analyzer was -140 dBm/Hz. A noise function option on the analyzer then gave us our result, at a frequency of 25 MHz, in dBm/Hz.

The dc current generated by the photodiode was measured in mA on a low noise, hand held multimeter. As will be discussed below, this dc current level was used to normalize our intensity noise measurements to the shot noise level (SNL) and as a reference for detector saturation.

#### Measurement of the Shot Noise Level

To normalize to the SNL, the noise power density of the laser was compared with that of a low quantum efficiency light emitting diode (LED). An LED is also a semiconductor which emits photons when pumped by an electrical current, but unlike a laser diode, it is not an optical resonator. (Quantum efficiency in this case means the ability of an electron, from the injection current to generate a photon.) There is no optical feedback and thus no stimulated emission; all the photons are spontaneously emitted. Although the light emitted by an LED does not have a well defined phase and therefore is not coherent light (see Shot Noise Limit in Ch. 1 of this thesis), the statistics of the randomly generated photons are Poissonian. The intensity noise of the LED is therefore at the shot noise limit (SNL).

The LED injection current was varied, and the noise power density at 25 MHz of the LED measured for different dc photodiode current levels. Because the dc photodiode current is proportional to the square root of the dc electrical power ( $P=I^2R$ ), and because the LED is shot noise limited, a plot of its noise power density vs. dc current yields a straight line (the noise power is proportional to  $(\Delta I)^2$  and  $(\Delta I)^2 \propto I$  from Eq. 1.2). This data is shown as '+'s in Fig. 3.3, and a least squares fit to these points shown by the solid line. The SNL of the laser, for a particular photodiode current level, is then found by multiplying its dc photodiode current level by the slope of this line.

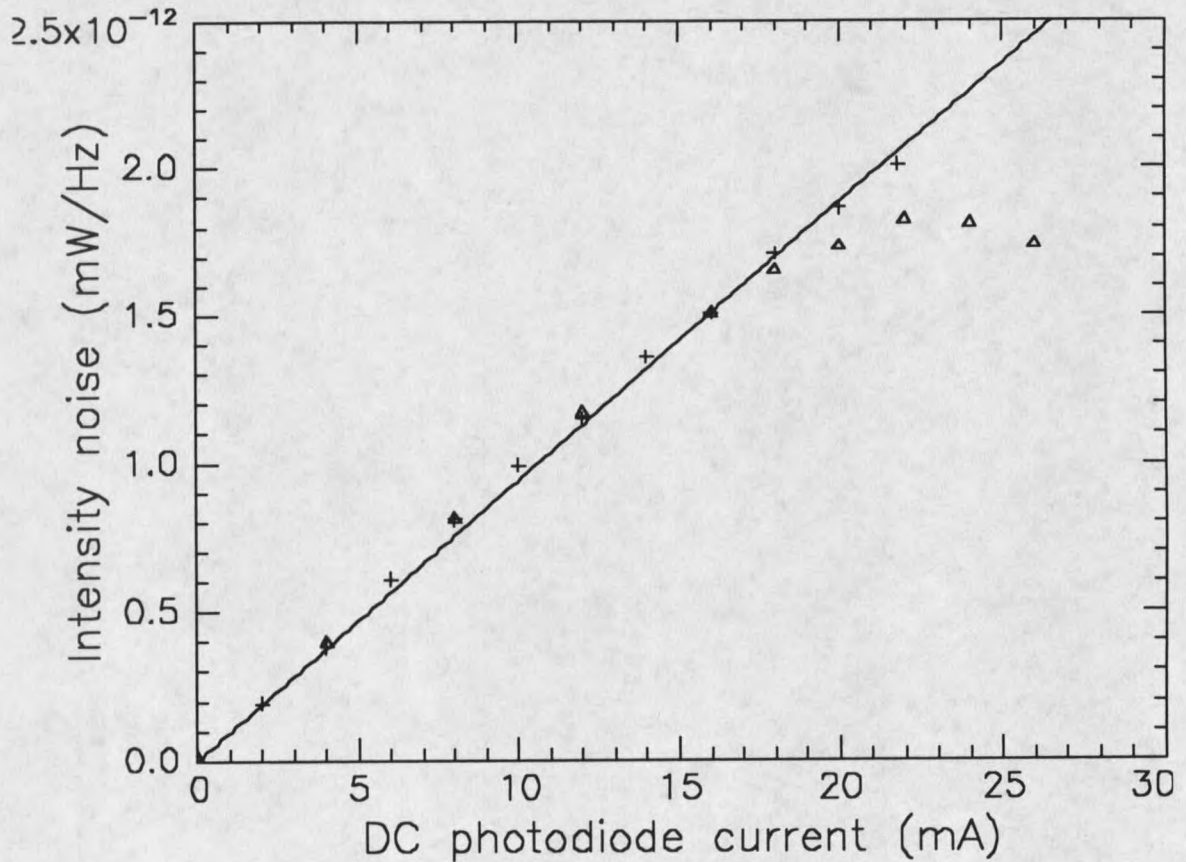


Figure 3.3. The shot noise of an LED at 25 MHz is proportional to the dc photodiode current, as shown by the '+'s. The triangles show the detector can saturate at 25 MHz if the beam is focused too tightly.

### Experimental Precautions Taken

To verify that thermal noise from the ILX current controller was not adding additional noise to the laser (and LED), two steps were taken. First, the intensity noise of the laser was measured using a well shielded battery and potentiometer circuit as a current source. At several injection currents intensity noise measurements were identical to those obtained with the ILX controller. Second, 40 mA of current from the ILX controller was sent directly through our cascaded amplifiers to the spectrum analyzer. The noise from the controller could then be compared with the calculated shot noise for this same amount of current. We found the noise of the controller current to be more than 10 dB below the SNL for the current.

The saturation properties of the photodiode were frequency dependent. To be sure that we were operating in the linear regime of the photodiode and the rest of the detection system, we did the following. The detector was placed at several different distances from the LED in order to vary the diameter, and therefore the intensity, of the beam impinging on it. Then, by varying the LED power (via the injection current) or using calibrated neutral density filters, we were able to determine the dc and ac saturation characteristics.

As shown in Fig. 3.4, the dc current of the photodiode remained linear with optical power to a dc current of over 24 mA. Data was taken for beam diameters of 2 mm and 10mm; both sets of data show the same "straight line". On the other hand, at 25 MHz the output of the detector did show saturation. The "shot noise" data from Fig. 3.3 illustrates this. (Note that because the current corresponding to dc saturation of the photodiode is higher than 24mA,

we plot the more convenient dc photodiode current on the horizontal axis in Fig. 3.3 instead of optical power). The +s, obtained with a beam diameter of 7.6 mm, show little saturation and have the constant slope associated with the SNL. The data shown by the triangles, however, were obtained with a beam diameter of 2.7 mm. At dc currents of about 18 mA the detector's ac response begins to saturate and the slope decreases. In this way we were able to determine an upper limit of the beam intensity for linear operation of the detection system at 25 MHz.

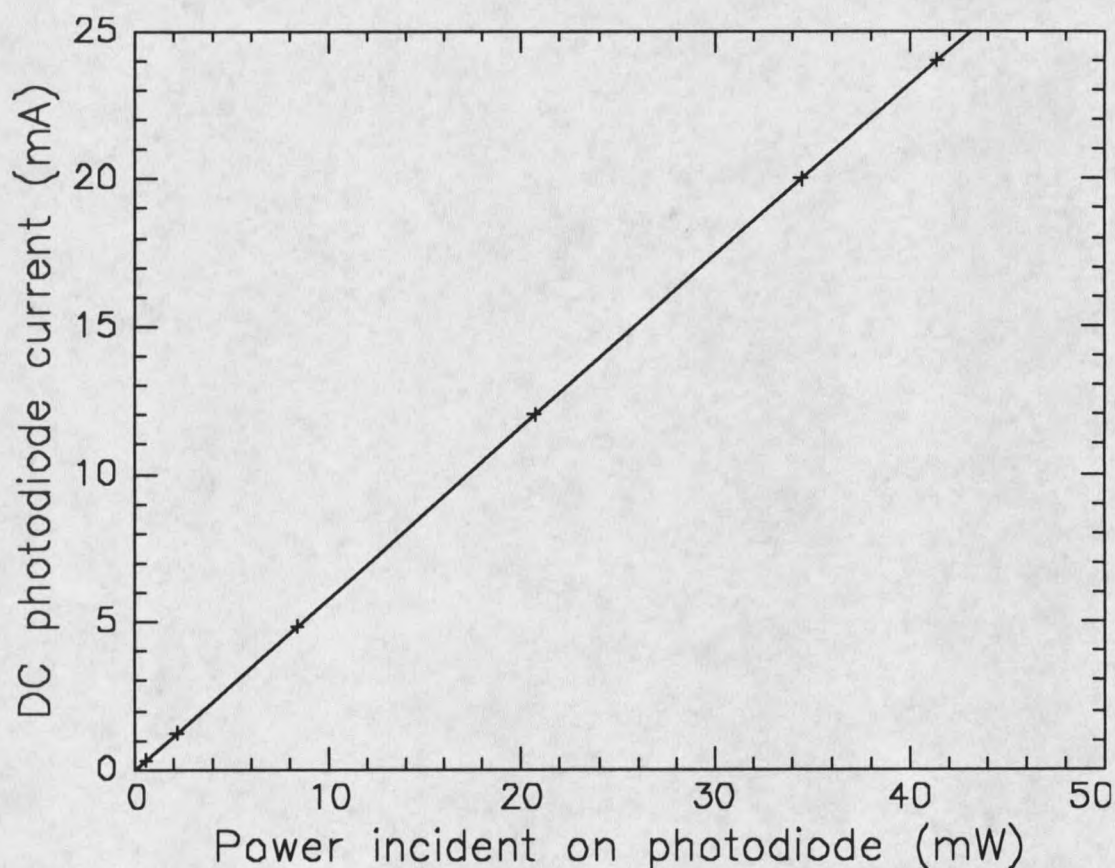


Figure 3.4. The dc output current of the photodiode is linear with optical power to up to a dc current of 24 mA.

For our experiment, dc photodiode currents were kept less than 15 mA and spot size diameters kept larger than 5 mm. In order to avoid the ac noise power saturation at higher

injection currents, the laser was placed such that 42% of the light spilled over the edges of the detector. This laser-detector coupling factor was then incorporated into the final results.

To insure that unwanted light scattered from the detector back into the laser did not affect the laser and thereby affect our noise measurements, the detector was placed at different distances and angles with respect to the laser (Fig. 3.2). In all cases identical results were obtained.

### Measurement of Laser Side Mode Suppression

An experiment was also performed to measure the laser mode suppression ratio (MSR), the ratio of the power in the main mode to that in the side modes, at injection currents where intensity noise measurements were taken. This was done not only to see how the intensity noise varied with MSR but also to select experimental data points to be modeled by the single mode theory. A MSR of 20 dB or higher was defined as single mode operation.

As shown in Fig. 3.4, an optical isolator, a spectrometer, and calibrated neutral density filters were used to measure the MSR. The optical isolator was needed to prevent stray reflections at the entrance slit of the spectrograph from being reflected back into the laser, and provided 25-30 dB of isolation at our lasing wavelength of 788 nm. The grating in the spectrometer spatially separated the longitudinal modes and the neutral density filters allowed us to examine the relative magnitudes of the longitudinal mode intensities. We were able to detect side modes which were 40 dB weaker than the main mode.

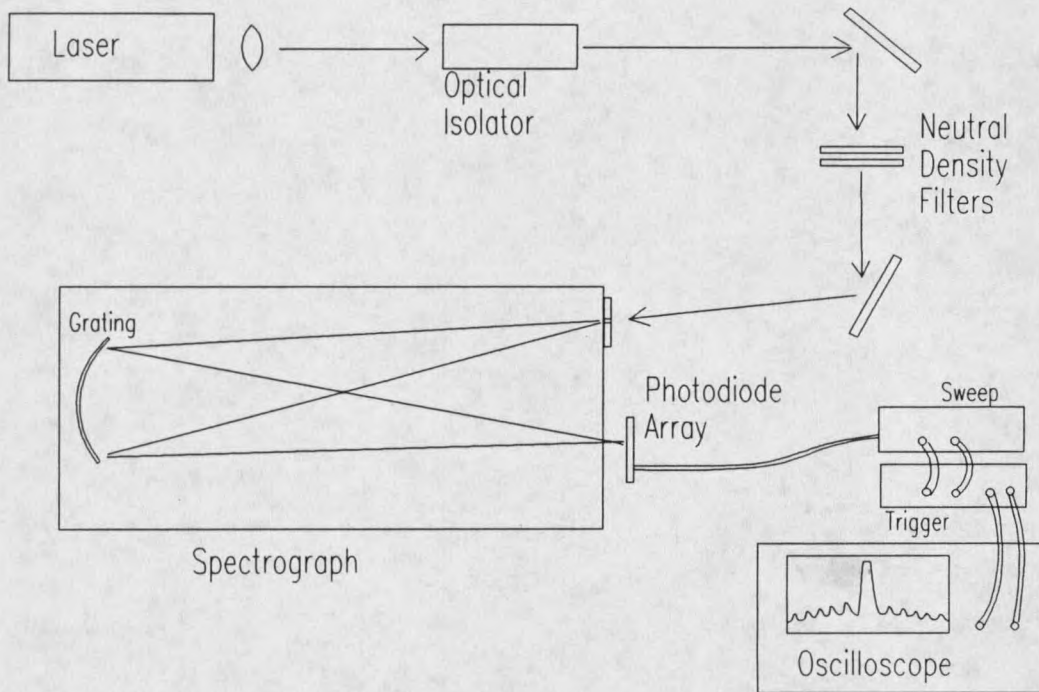


Figure 3.5. Experimental setup used to measure the longitudinal side mode suppression.

### Results

The intensity noise normalized to the SNL,  $S_o(\omega)/S_{SNL}$ , is shown as '+'s in Fig. 3.6. Near threshold ( $R \approx 0$ ) the intensity noise is 25 dB above the SNL, while at twice threshold ( $R=1$ ), it is 5 dB above the SNL. Also plotted as a solid line in Fig. 3.6 is the MSR; it ranges from 0 to 28 dB, generally increasing with injection current. At  $R=0.42$  longitudinal "mode hopping" occurred. Mode hopping is a form of mode partitioning, but instead of a partial

exchange of power amongst many modes, full exchanges of most of the laser power occur between just two modes. A correlation between intensity noise and MSR is evident here.

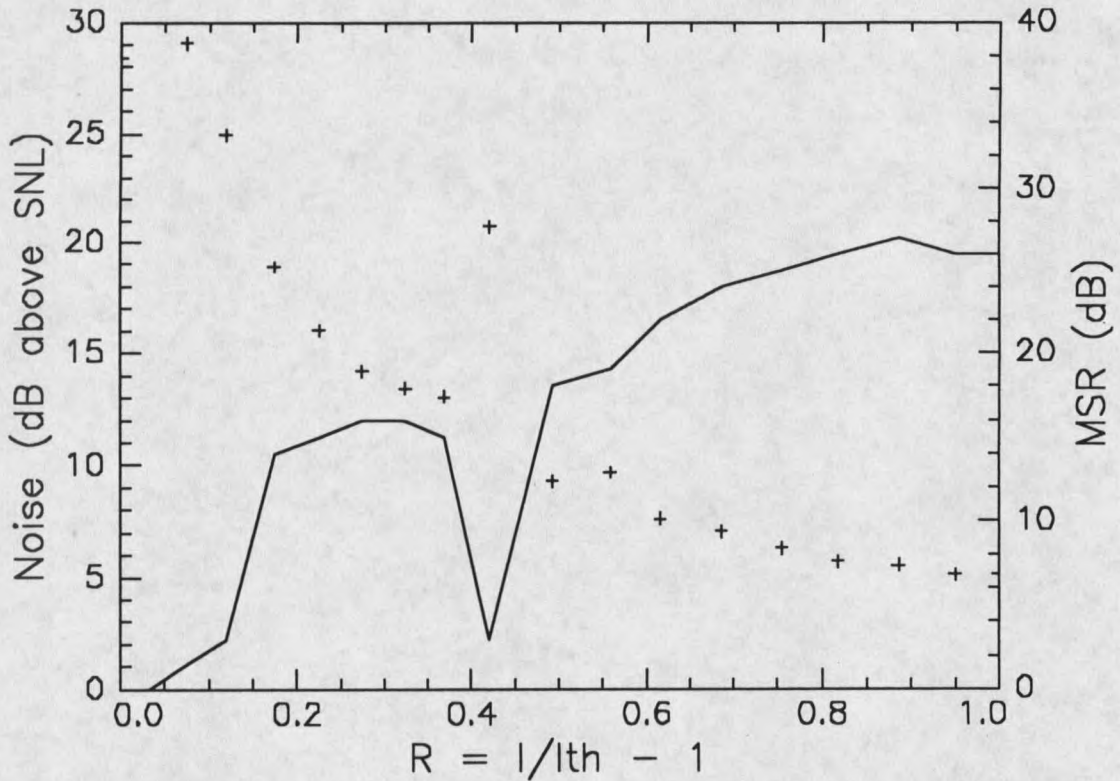


Figure 3.6. The intensity noise and MSR plotted as a function of the normalized injection current. ( $R=0$  corresponds to threshold and  $R=1$  to twice threshold).

In Fig. 3.7 the quantum and semiclassical theories, with the pump noise set to zero, are plotted with our experimental intensity noise data. The parameters used in the theory are derived or referenced in Appendix B. At  $R=1$ , the experimental intensity noise is 3 dB above the quantum theoretical prediction and 7 dB above the semiclassical theoretical prediction. Although the two theories agree at low injection currents, the measured intensity noise is even

further above the theoretical predictions here. As one would expect, neither single mode theory models the mode hopping behavior at  $R=0.42$ .

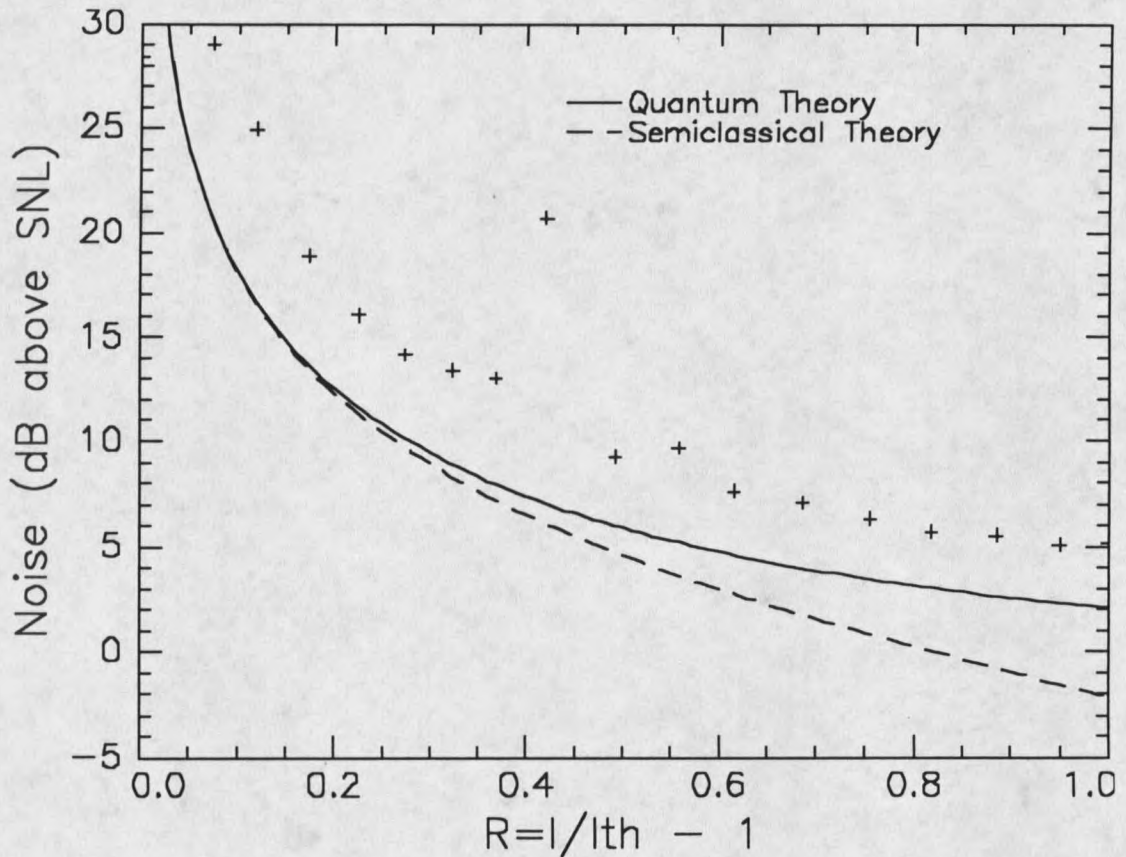


Figure 3.7. The quantum theory (solid line) and semiclassical theory (dashed line) shown with our experimental intensity noise data (+'s).

### Discussion

We believe that noise due to the longitudinal side modes is increasing our intensity noise measurements above that which is predicted by the two single mode theories. First, the intensity noise increases sharply when the laser begins to "mode hop". Second, although the theories predict high levels of relaxation oscillation noise at low injection currents, we still

measure more noise than the theories predict. The MSR is low, and therefore the noise due to mode partitioning is large and not completely dominated by relaxation oscillation noise. Finally, at higher injection currents where the MSR is larger (and therefore the effects of the side modes smaller), intensity noise measurements, although still high, come closer to theoretical predictions.

## CHAPTER 4

### EXTERNAL CAVITY SEMICONDUCTOR LASER

An external cavity (EC) semiconductor laser is one in which optical elements are placed external to a laser diode, in order to modify the laser cavity and enhance its performance. Three properties which make the EC laser more attractive for a variety of applications include a narrow linewidth, tunability, and most relevant to this thesis, a high side mode suppression. Providing optical feedback at a small range of frequencies around a longitudinal mode frequency of the diode helps that mode to lase more strongly at the expense of its side modes.

The experimental setup and procedure for measuring the intensity noise of the EC laser is similar to that for the free running laser (Ch. 3). Only the differences in the experimental procedure will be presented here. The semiclassical and quantum theoretical expressions are again used to model the intensity noise. (Modifications in theoretical parameters for the two different lasers are discussed in Appendix C). This fourth chapter provides further verification of the conclusions reached in Chapter 3.

### External Cavity Laser

Figure 1 shows a schematic of the grazing incidence (or Littman-Metcalf)<sup>33</sup> external cavity (EC) semiconductor laser used in this second experiment. A diffraction grating was placed at a grazing incidence angle with respect to the beam emerging from the laser diode of Chapter 3. The first order diffracted beam was sent back into the laser via the mirror. Because the frequency components of the light were spread spatially by the grating, only a small range of optical frequencies were sent back into the diode. The specular reflection (zeroth order beam) from the grating then became the EC laser output.

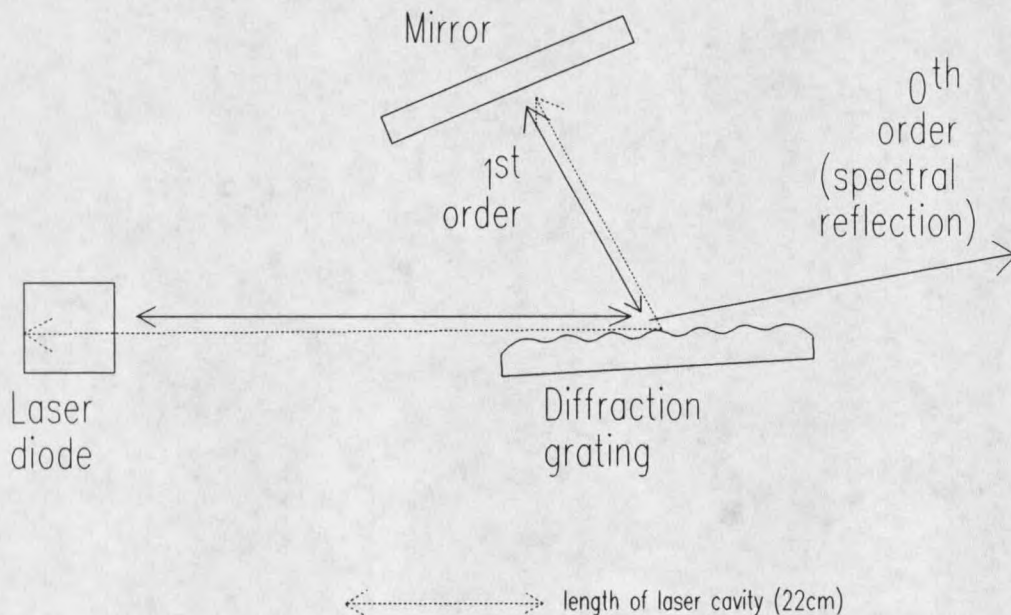


Figure 4.1. Schematic of the EC semiconductor laser. The diode itself is the one discussed in Chapter 3.

The amount of optical feedback provided by the grating and mirror was much higher than that of the front surface of the diode. In the EC laser 11% of the diode's output was reflected back into the diode, compared with 0.65% in the free running case (just the solitary diode). The effective cavity length was the distance the light traveled from the back surface of the diode to the mirror as shown in Fig. 4.1. Due to the residual reflectivity of the front surface of the diode however, its longitudinal modes still played a role as will be discussed below.

A more detailed look at the EC laser is provided by Fig. 4.2. A Thor Labs single element aspheric lens at the output of the diode collimated the beam. The lens, which had a numerical aperture of 0.55, was held in place by a flexure mount machined "in house" by Gregg Switzer. The holographic gold plated grating, made by Spectragon, had 1800 lines per mm. It was placed at a grazing incidence angle of  $86.5^\circ$  with respect to the beam emerging from the diode. The grating, mirror, and lens were all coated to minimize absorption losses 788 nm.

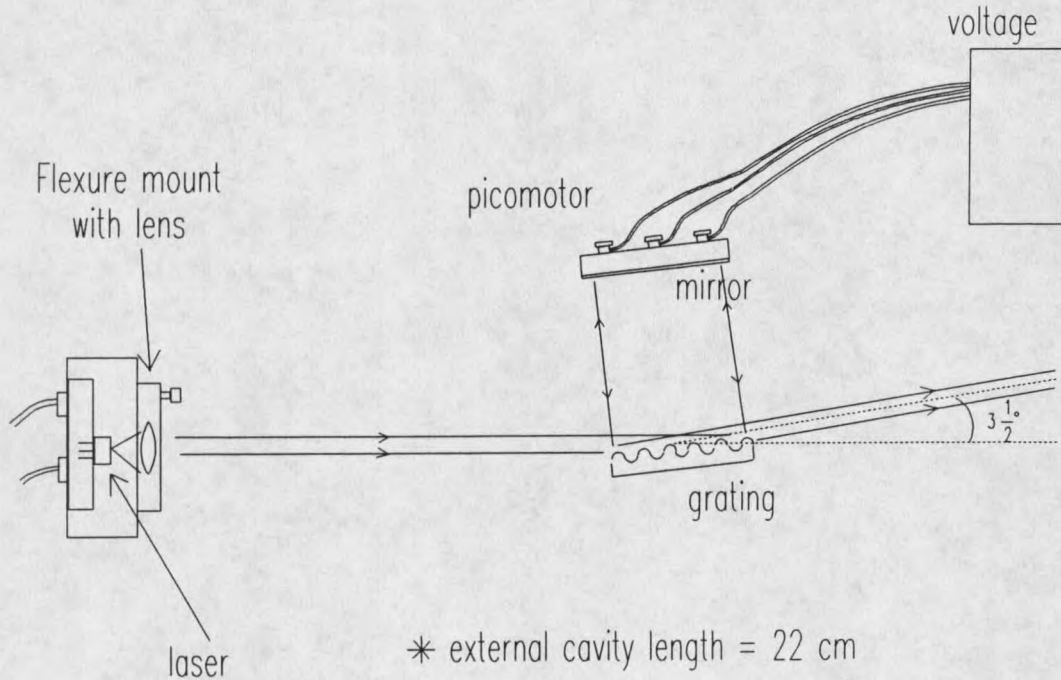


Figure 4.2. Details of the grazing incidence EC laser used in this second experiment

The angular dispersion of the grating was such that a range of wavelengths  $\Delta\lambda=0.002$  nm (or  $\Delta\nu=1$  GHz) was reflected back into the diode. The spacing between the longitudinal modes of the diode was 0.213 nm (103 GHz), and just one longitudinal mode of the free running laser received external optical feedback.

The wavelength of an EC laser can be tuned due to the broad gain profile of a diode laser (see Semiconductor Basics in Ch. 1 of this thesis). This was done both by rotating the mirror, such that a different wavelength of light from the grating is sent back into the laser, and by translating the mirror, to change the cavity length. The mirror was mounted on a New Focus multi-axis picomotor driver. The picomotor had an angular

resolution of 2 milliradians; this allowed us to change the wavelength of the laser in 0.05nm increments. The picomotor had a translational resolution of 100 nm; this allowed us to fine tune the laser's wavelength by  $4 \times 10^{-4}$  nm increments (or better than one part in  $10^6$ ; more than ample resolution).

Longitudinal modes of the solitary diode still existed because of the 0.65% reflectivity of the front surface of the diode. To minimize the effects of the diode modes, the EC lasing wavelength was tuned to match one of the longitudinal modes of the solitary diode. Fig. 4.3 illustrates this. At each injection current where intensity noise measurements were taken, the mirror was adjusted (by both rotation and translation) to optimize the output power. A maximized output power corresponded both to the EC laser lasing at a the center wavelength of a solitary diode mode and the highest MSR.

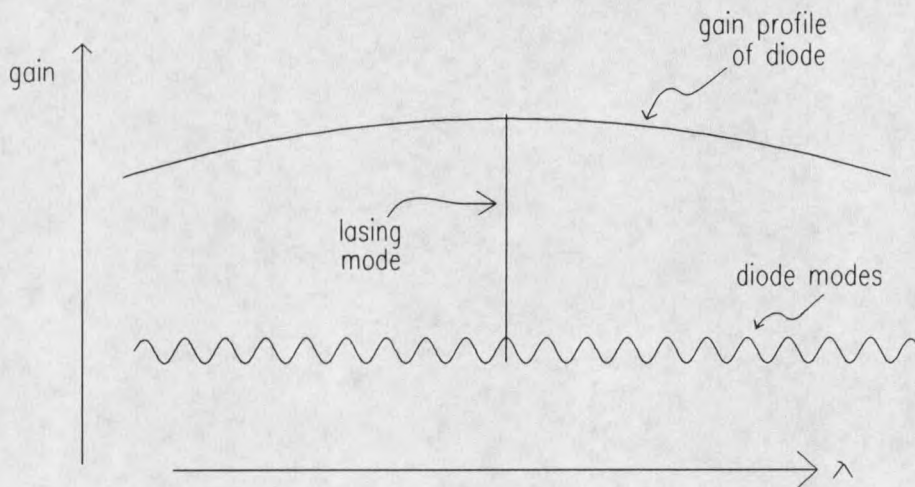


Figure 4.3. The wavelength of the EC laser had to be at a resonant wavelength of the solitary laser diode.

Experimentally measured power versus injection current curves for the EC laser and the free running laser are shown in Fig. 4.4. The threshold current of the EC laser is 50 mA, 10.5 mA below that of the free running laser. The slope of the curve for the EC laser is half of that for the free running laser. This is discussed in Appendix C where the slope of the free running laser's power vs. injection current curve is used to determine several theoretical parameters.

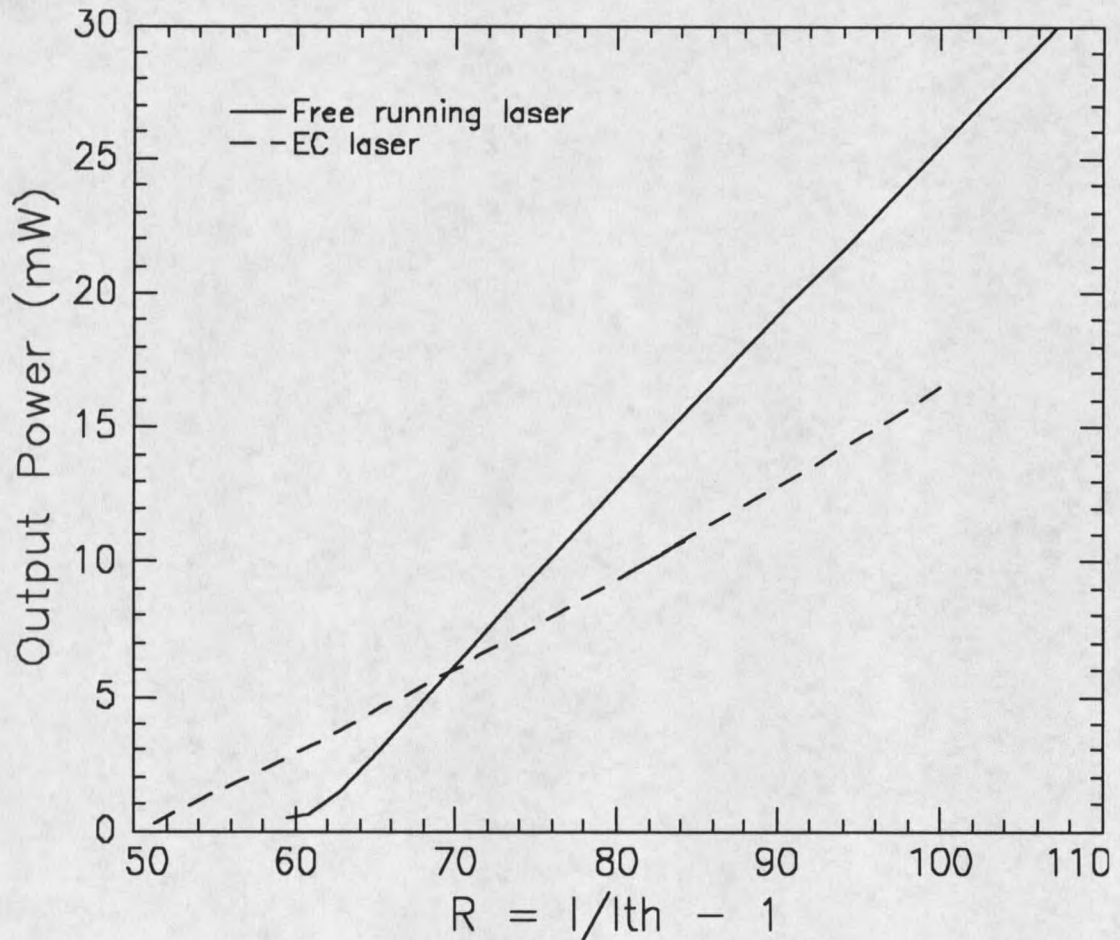


Figure 4.4. Output power vs. injection current plots for the free running and EC lasers.

## Experiment

Except for the addition of an off-axis parabolic mirror, the experimental setup for measuring the intensity noise of the external cavity laser was identical to that used to measure the intensity noise of the free running laser. The off-axis mirror was used to expand the EC laser's collimated beam, to avoid saturation at the detector. (A lens used for this purpose would have reflected some light back into the laser.) As in the first experiment 42% of the beam spilled over the edges of the detector. The mode suppression ratio was also measured as in the first experiment.

## Results

Figure 4.5 shows the measured intensity noise and side mode suppression ratio (MSR) as a function of injection current. At twice threshold ( $R=1$ ), the intensity noise is 2 dB above the SNL and 3 dB below that of the free running (Fig. 3.6). Just above threshold, the intensity noise falls sharply and the MSR rises rapidly. This is in contrast to the rise and fall of the intensity noise and MSR for the free running laser (Fig. 3.5), which changed with injection current much more gradually.

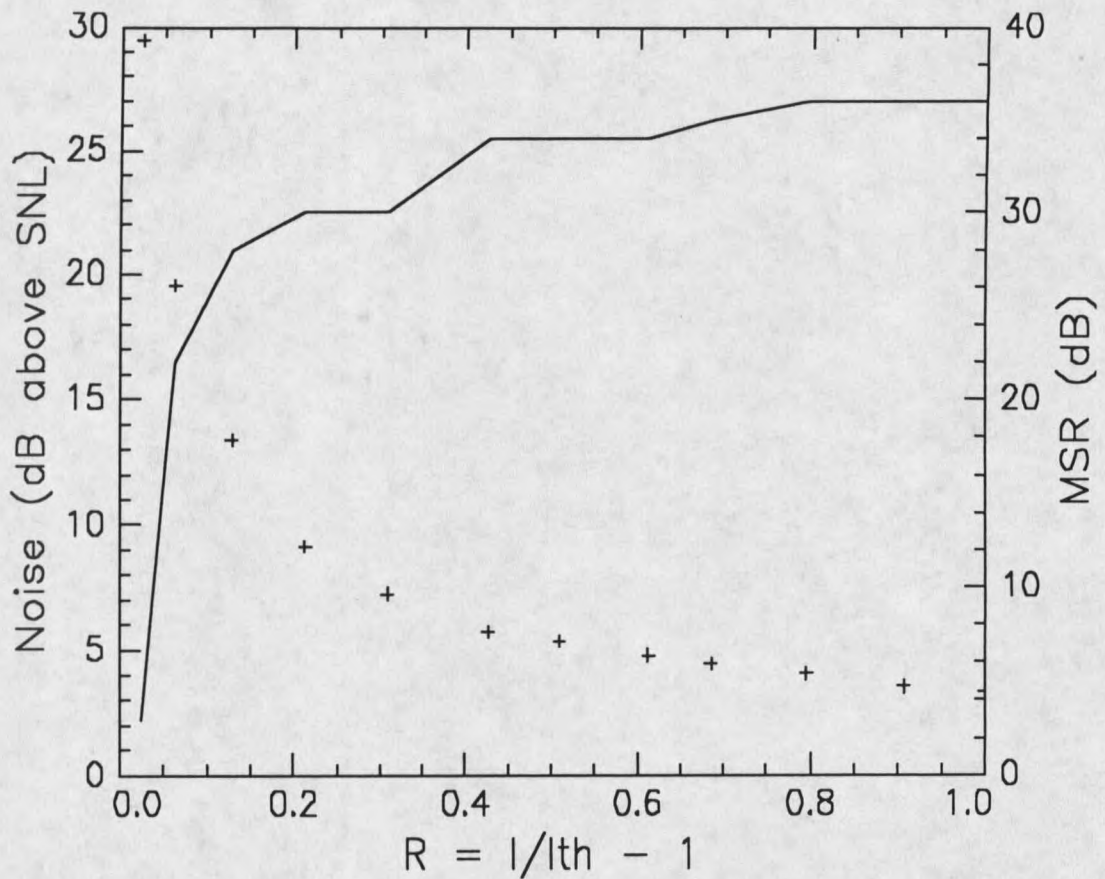


Figure 4.5. The intensity noise and MSR both plotted as a function of the normalized injection current.

As shown in Fig. 4.6 both the semiclassical and quantum theories are again below the intensity noise data, the semiclassical theory more so than the quantum theory. At twice threshold ( $R=1$ ), the measured intensity noise is 2.5 dB above the quantum theory, and 5.5 dB above the semiclassical theory.

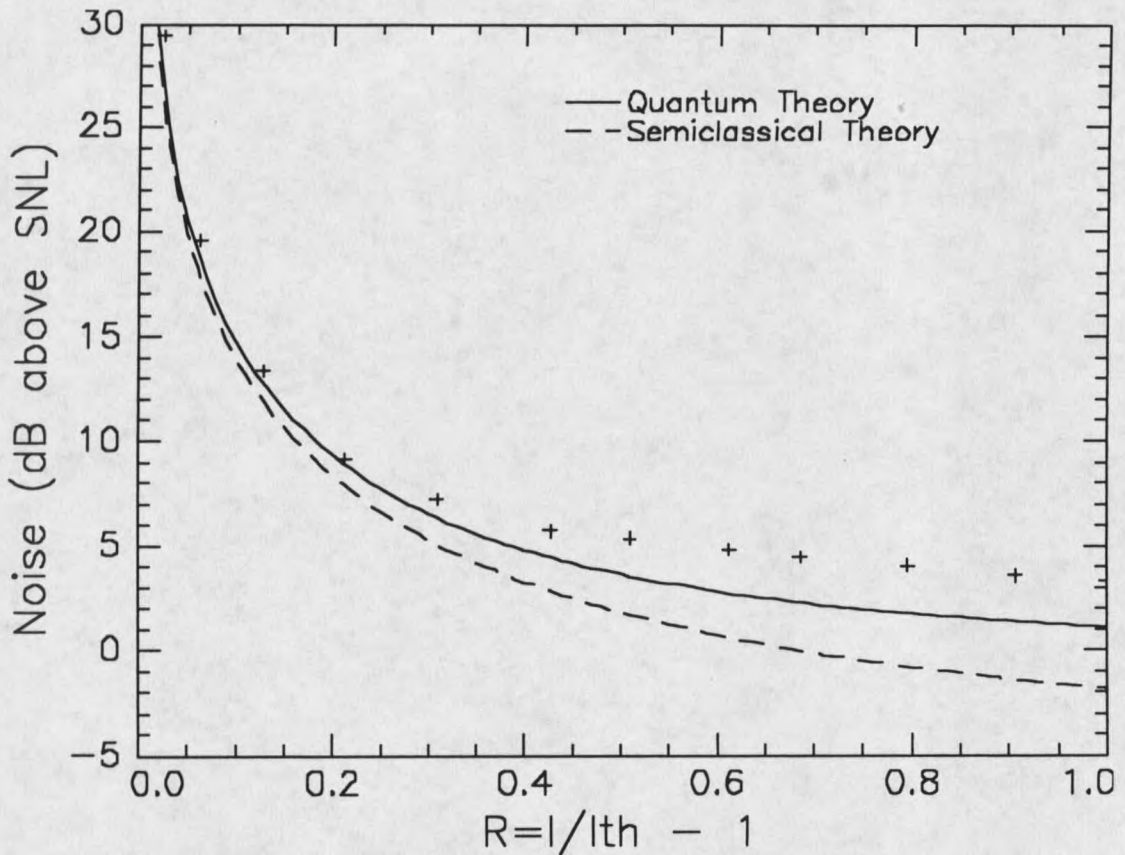


Figure 4.6. The experimental EC laser intensity noise data (+'s) shown with the quantum theory (solid line) and semiclassical theory (dashed line).

### Discussion

Unlike the free running laser, the MSR of the EC laser is high at low injection currents. Therefore at low injection currents the noise due to the longitudinal side modes is small, and the noise predicted by the theories is close to that of our experimental data. (The single mode theory only predicts relaxation oscillation noise and not noise due to the longitudinal side modes.) We believe that at larger injection currents, although the MSR is high, longitudinal side mode noise still contributes significantly to the overall noise. This

is because at high pump rates noise due to relaxation oscillations is small. Thus, as for the free running laser of Chapter 3, our intensity noise measurements lie above the single mode theoretical predictions at high injection currents.

## CHAPTER 5

## CONCLUSION

Simple semiconductor laser configurations can produce light with low levels of intensity noise in the frequency range 1-100 MHz. In particular we measured the intensity noise at 25 MHz, of both an "off-the-shelf" laser diode and an external cavity laser diode. At injection currents of twice threshold, the intensity noise of the solitary laser diode was 5 dB above the shot noise level (or standard quantum limit), and the intensity noise of the external cavity laser diode was just 3.5 dB above the shot noise level.

We found the fully quantum mechanical theory based on the Langevin rate equations, to model our intensity noise data better than that of the semiclassical theory (also based on Langevin rate equations). However, our experimental intensity noise measurements were in general larger than the noise levels predicted by either single mode theory. Although at high pump rates the side modes were as much as 35 dB below that of the main mode (in the external cavity laser case), we believe that this "extra" noise is due to the presence of the longitudinal side modes. A multimode theory needs to be employed to more precisely model the intensity noise of these lasers.

**APPENDICES**

APPENDIX A  
CONTROLLER NOISE

In this appendix, noise spectra are presented for two different commercial controllers, as well as for a well shielded battery supply. Examples are also given to show the sensitivity of the noise level to small changes in wiring and grounding procedures. The experimental setup used to obtain noise spectra is similar to that discussed in Chapters 3 and 4. The magnitude (or units) for the intensity noise in the spectra here, however, is given in terms of the quantity "relative intensity noise".

### Relative Intensity Noise (RIN)

Relative intensity noise, or RIN, is defined as

$$RIN = 10 \text{Log} \frac{\langle \Delta P \rangle^2}{\langle P \rangle^2}, \quad (\text{A1})$$

where  $\langle \Delta P \rangle^2$  is the mean square optical intensity fluctuation in a 1 Hz bandwidth at a particular frequency and  $\langle P \rangle^2$  is the mean-square average power.<sup>27</sup> The units for RIN are therefore dB/Hz. Since electrical power  $\propto$  (optical power)<sup>2</sup>, when a photodiode is used to detect the light, RIN is actually the ratio of two electrical powers.

### Intensity Noise Spectra

Figures A.1, A.2, and A.3 show intensity noise spectra for a diode laser, over three different frequency ranges, using different current sources to pump the laser. Controller A

(the ILX-3722) was the more sophisticated of the two commercial controllers, with options for remote GPIB operation and temperature control. The laser pumped with this controller had the highest RIN in the frequency range 1-150 MHz. Controller B (the ILX-3620) was a lower cost controller, with fewer options for the user. The laser pumped by it had the highest RIN below 1 MHz. The battery supply contained a 6 volt alkaline battery with a resistor in series (Fig. A4). It gave the lowest noise spectra over all three frequency ranges.

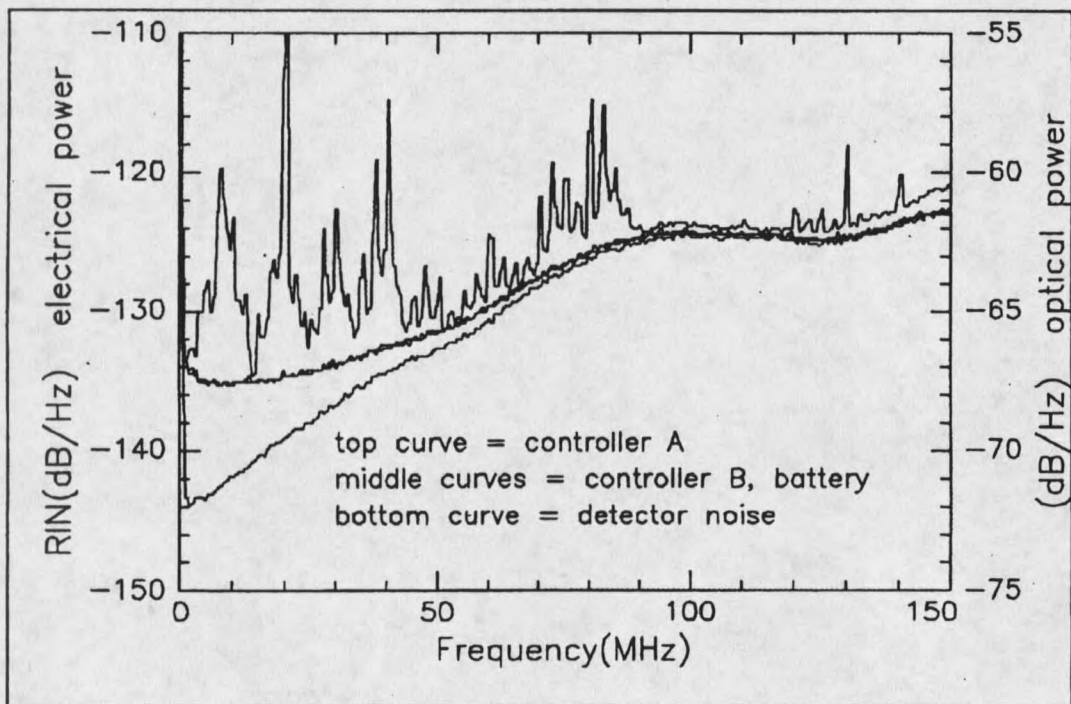


Figure A.1. The RIN of the laser pumped by controller A (ILX-3722) has the RIN in the frequency range 1-150 MHz.

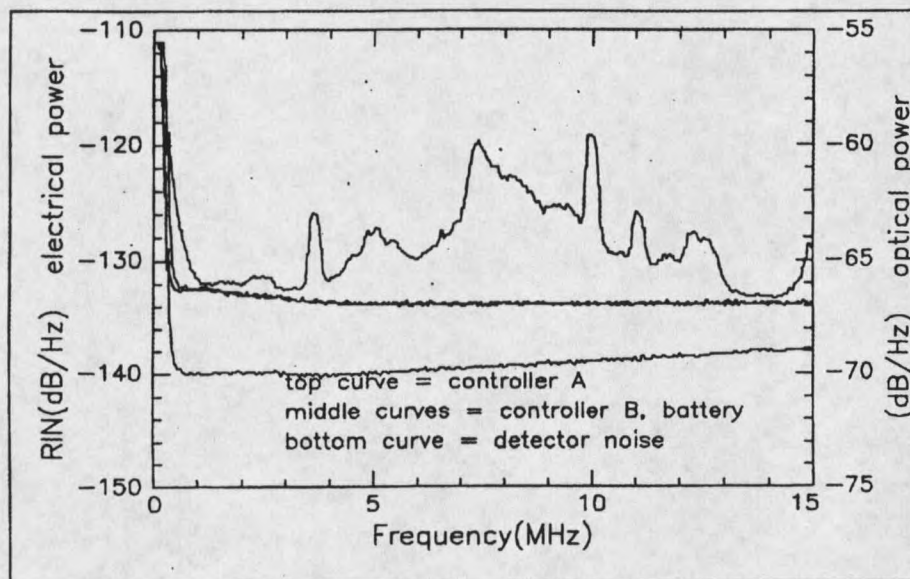


Figure A.2 (above). The RIN of the laser pumped by controller A (ILX-3722) is highest in the frequency range 1-150 MHz.

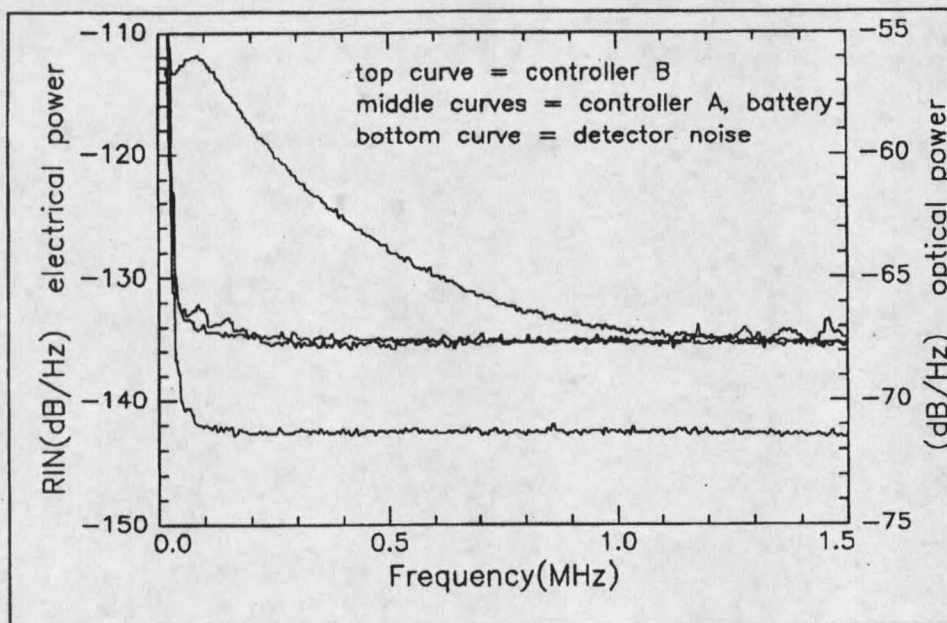


Figure A.3 (above). The RIN of the laser pumped by controller B (ILX-3722) is highest at frequencies below 1 MHz.

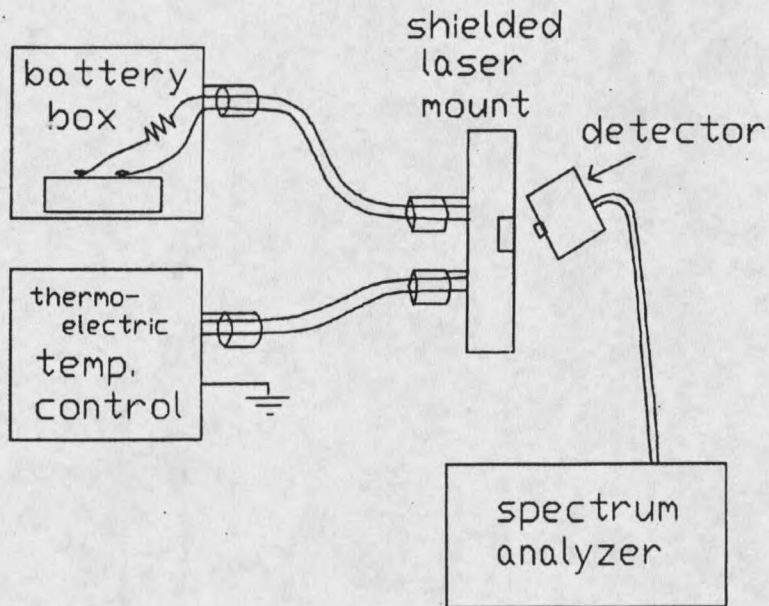


Figure A.4. This experimental configuration, with the laser pumped by a well shielded battery box, gave us the lowest RIN.

Figure A.5 shows two setups with a GPIB cable connected to controller A. In setup 1 the GPIB cable case is insulated from the controller (as it should be) and in setup 2. the GPIB cable case is connected to the controller. From the spectrum in Fig. A.6, we see that there is a significant increase in the intensity noise for setup 2.

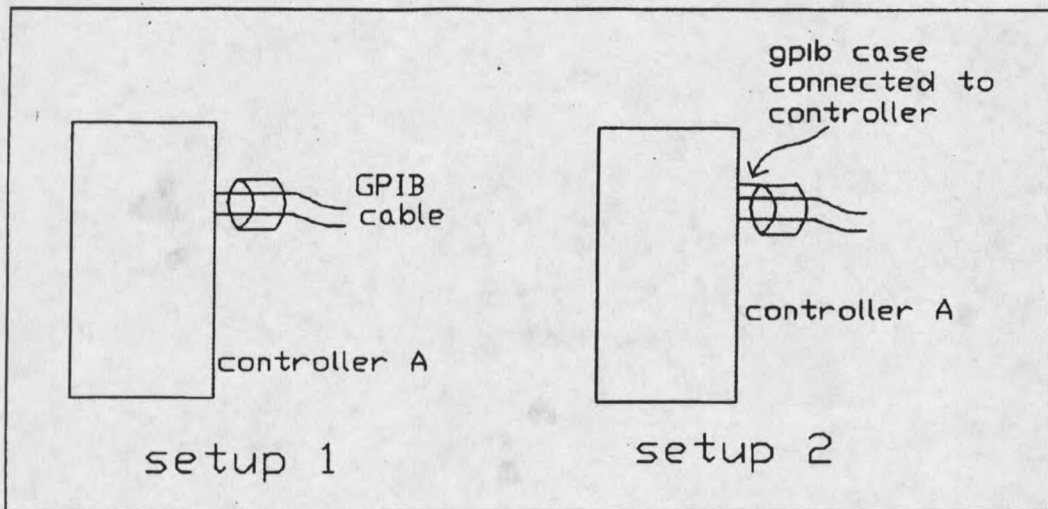


Figure A.5. In setup 1 the case of the GPIB cable (used for remote operation of the controller) is insulated from the controller. In setup 2 the GPIB case is connected to the controller.

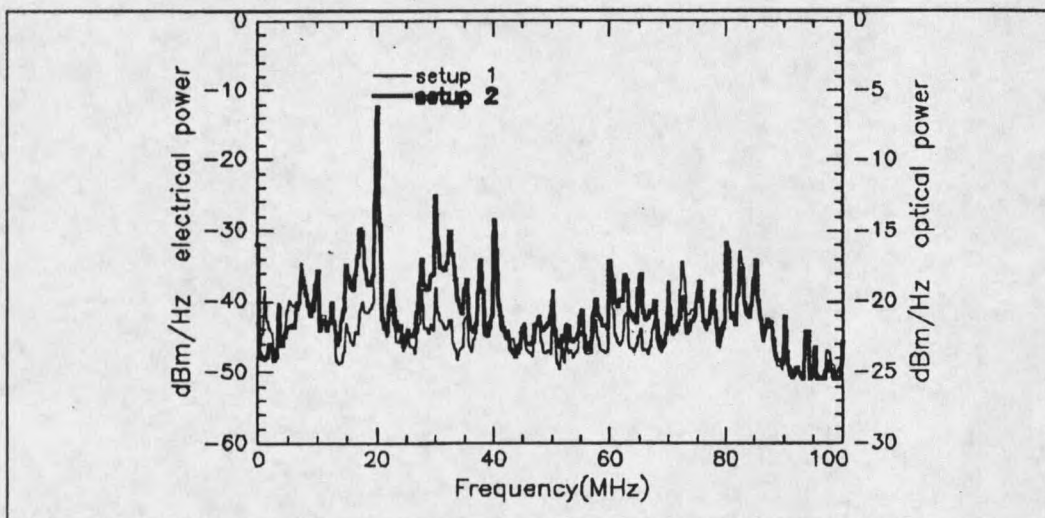


Figure A.6. The laser shows significantly more noise when powered by the configuration in setup 1 than by the configuration in setup 2.

APPENDIX B  
LASER PARAMETERS

The parameters used in the semiclassical and quantum theories, for both the free running and external cavity lasers, are given in this appendix. Where appropriate we explain the procedure used in obtaining the parameters. Some parameter values, in particular the front and back surface reflectivities of the laser, were obtained from a Sharp representative, Dr. Herb Moeller.<sup>34</sup> (He in turn obtained the parameter values from Sharp, Inc. in Japan.) Because parameters can vary from laser to laser however, the values given to us by Dr. Moeller could be conservative estimates of the true or typical value.

#### Free Running Semiconductor Laser

The threshold injection current  $I_{th}$  is used in the calculation of many laser parameters. It is determined experimentally from the power vs. injection current plot for the free running laser (Fig. 4.4) to be 60.5 mA.

The index of refraction  $n$  and the group index of refraction for the inverted active region  $n_g$  are needed to determine the group velocity of the light inside the active region. The index of refraction  $n$  can be determined from existing data given for AlGaAs. Figure 2.6 of reference [35] shows the mole fraction of  $Al_xGa_{1-x}As$  at  $\lambda = 788$  nm to be  $x = 0.12$ .<sup>34</sup> Using this mole fraction, Fig. 2.5-4 of reference [36], which gives the index of refraction vs. the mole fraction, can be used to obtain  $n=3.60$ . The group index of refraction  $n_g$  for an inverted medium is approximated by

$$n_g = n - \nu \frac{\partial n}{\partial \nu} \quad (\text{B.1})$$

with  $\nu$  the frequency of the laser light. The partial derivative  $\frac{\partial n}{\partial \nu}$  is estimated from Fig.

2.5-4 of reference [36] to be  $-10^{-15}$  for  $\lambda = 788$  nm. Then with  $\nu = 3.8 \times 10^{14}$ ,  $n_g$  becomes

4.0.

Next we determine the gain rate  $G$  and the photon loss rate  $\frac{1}{\tau_p}$ , which are equal

above threshold. The photon loss-rate is the sum of both internal and external loss rates,

$$G = \frac{1}{\tau_p} = \frac{1}{\tau_e} + \frac{1}{\tau_i} \quad (\text{B.2})$$

The photon loss rate through both output ports is determined from the reflectivities of the output ports as<sup>27</sup>

$$\frac{1}{\tau_e} = \frac{v_g}{2L} \ln \left( \frac{1}{R_1 R_2} \right), \quad (\text{B.3})$$

where  $v_g$  is the group velocity of the light in the laser medium  $\left( \frac{c}{n_g} \right)$ ,  $L$  is the length of the

laser cavity, and  $R_1$  and  $R_2$  are the reflectivities of the front and back surfaces of the laser,

respectively. The front and back reflectivities of the laser were given to us by Dr. Dave

Moeller<sup>34</sup> as 6% ( $R_1 = 0.06$ ) and 90% ( $R_2 = 0.9$ ) respectively. The length of the laser

cavity was also given to us by Dr. Moeller as 300  $\mu\text{m}$ . The loss rate through both output

ports  $\frac{1}{\tau_e}$ , then becomes  $3.65 \times 10^{11}/\text{s}$ .

Once the external photon loss rate is known, the internal photon loss rate (due to carrier scattering and carrier absorption) can be found from the slope of the output power vs. injection current plot (Fig. 4.4). The slope is proportional to the differential or external quantum efficiency<sup>37</sup>

$$\eta_d = \eta_i \frac{\left(\frac{1}{\tau_e}\right)}{\left(\frac{1}{\tau_e} + \frac{1}{\tau_i}\right)}, \quad (\text{B.4})$$

where  $\eta_i$  is the internal quantum efficiency. The internal quantum efficiency represents the fraction of carriers that recombine radiatively and is taken to be 1 above threshold.<sup>37</sup> To use the power vs. injection current plot in Fig. 4.4 we relate the output power to the differential quantum efficiency by the expression

$$P_o = C \frac{\hbar\omega}{q} \eta_d (I - I_{th}). \quad (\text{B.5})$$

Here  $C$  is the fraction of the output power which is coupled out of the laser through the front facet. Using the slope of the power vs. injection current plot for the free running

laser in Fig. 4.4,  $C = \frac{0.94}{0.94 + 0.10}$ , and Eqs. (B.4) and (B.5), we obtain  $\frac{1}{\tau_i} = 1.2 \left(\frac{1}{\tau_e}\right)$  or

$\frac{1}{\tau_i} = 4.38 \times 10^{11}/\text{s}$ . The internal and external loss rates are then added (Eq. D2) to obtain

a gain  $G$  of  $8.03 \times 10^{11}/\text{s}$ .































